Journal of Fluids and Structures 42 (2013) 401–420

Contents lists available at ScienceDirect

Journal of Fluids and Structures

journal homepage: www.elsevier.com/locate/jfs

One and two degrees-of-freedom Vortex-Induced Vibration experiments with yawed cylinders

G.R. Franzini [a,*], R.T. Gonçalves [b], J.R. Meneghini [a], A.L.C. Fujarra [b]

[a] NDF – Fluids and Dynamics Research Group, POLI, University of São Paulo, Brazil
[b] TPN – Numerical Offshore Tank, POLI, University of São Paulo, Brazil

ARTICLE INFO

Article history:
Received 18 September 2012
Accepted 20 July 2013
Available online 20 August 2013

Keywords:
Vortex-Induced Vibration
Experiments
Yawed Cylinders

ABSTRACT

Vortex-Induced Vibration (VIV) experiments were carried out with yawed cylinders. The purpose was to investigate the validity of the Independence Principle (IP) for properly describing the flow characteristics and the dynamics of structures subjected to oblique flow. Five yaw angles in relation to the direction perpendicular to the free stream velocity were tested, namely $\theta = 0^\circ$, 10°, 20°, 30° and 45°. Both the upstream and downstream orientations were tested. The models were mounted on a leaf spring apparatus that allows experiments with one or two degrees of freedom. The Reynolds numbers based on the component normal to the cylinder axis fell in the interval $3 \times 10^3 < \mathrm{Re_n} < 1.5 \times 10^4$. The mass ratio parameter was $m^* = 2.6$ and the cylinder aspect ratio was $L/D \approx 13$ for all the experiments. Time histories of displacement and hydrodynamic forces were acquired. Considering only the component of the free stream which is normal to the cylinder axis, the results of amplitude and force coefficients agreed reasonably well with the non-yawed ones for yaw angles up to 20° for both one and two degrees-of-freedom experiments. This indicates the validity of the IP for this yaw angle range. For yaw angles larger than 20°, a decrease in the maximum amplitude was observed. The decrease in the oscillation amplitudes was related to a larger modulation in the phase shift between force and displacement. Differences in the results for upstream and downstream were observed and were more evident for the larger yaw angle. These differences can be associated to the asymmetric cylinder end conditions.

1. Introduction

The flow around a fixed circular cylinder is one of the most studied problems within the fluids mechanics theme. In this case, the adverse pressure gradient leads to flow separation and, consequently, to the formation of two free shear layers. According to the model proposed in Gerrard (1966), the interaction between these free shear layers gives rise to the periodic vortex shedding process with a well-defined frequency f_s. A comprehensive discussion of the physics behind the flow around a fixed cylinder and the relationship between force coefficients (and Strouhal number St) and the Reynolds number Re can be found in the papers by Norberg (2001, 2003).

Even in the case of a fixed and non-yawed cylinder, oblique vortex shedding is also observed and accounts for the discontinuity at the Re × St plot at low Re values, as pointed out by Williamson (1989) and Hammache and Gharib (1991). Moreover, Williamson (1989) showed that the Strouhal curve for oblique shedding, St_α, can be collapsed onto the parallel

* Corresponding author. Tel.: +55 11 9 91981220.
E-mail addresses: gfranzini@usp.br, guilherme.franzini@gmail.com (G.R. Franzini).

0889-9746/$ - see front matter © 2013 Elsevier Ltd. All rights reserved.
http://dx.doi.org/10.1016/j.jfluidstructs.2013.07.006

shedding St_0 by using $St_0 = St_\alpha / \cos\ \alpha$, where α is the angle of vortex shedding. Both papers discussed the sensitivity of the vortex shedding angle with the end conditions.

On the other hand, if the cylinder is free to oscillate, the vortex shedding process can be severely affected, as pointed out in the reviews by Bearman (1984, 2011). Considering the problem of a rigid cylinder mounted on an elastic support with natural frequency f_N, the lock-in range is the one in which $f_s \approx f_N$.

As a resonant phenomenon, Vortex-Induced Vibration (VIV) presents the highest values of amplitude (order of one diameter) in the range of reduced velocity, $V_R = U_\infty / f_N D$ (U_∞ is the free stream velocity and D is the structural diameter), in which the lock-in is observed. The papers by Sarpkaya (2004), Gabbai and Benaroya (2005), and Williamson and Govardhan (2004, 2008) represent comprehensive reviews regarding the VIV phenomenon.

Up to the 2000s, the VIV investigations were focused on the problem of a rigid cylinder assembled onto an elastic base free to oscillate just in the direction transversal to the free stream (cross-flow direction). Defining the mass parameter as $m^* = m_s / m_d$ (m_s is the structural mass and m_d is the mass of fluid displaced by the body) and the damping ratio $\zeta = c / 2\sqrt{k(m_s + m_a)}$ (c is the structural damping, k is the stiffness and m_a is the potential added mass), the mass-damping parameter $m^*\zeta$ characterizes not only the maximum amplitude of oscillation (see Govardhan and Williamson, 2006), but also the aspect of the response curve.

Considering a system with low $m^*\zeta$, the amplitude plot can be split into initial, upper and lower branches. Each of these branches presents particular characteristics of amplitude/frequency of oscillation, hydrodynamic force coefficients and vortex shedding patterns. Further details regarding these aspects can be found in Khalak and Williamson (1997, 1999).

Motivated by the new technological demands, numerous investigations with a rigid cylinder free to oscillate simultaneously in both the in-line and cross-flow directions have been carried out. In this scenario, one of the most striking results indicates that the in-line oscillations strongly affect the cross-flow amplitude only if $m^*\zeta$ is below a specific value. This value depends on the experimental setup (see, for example, the parametric investigations carried out by Stappenbelt and Lalji, 2008; Blevins and Coughran, 2009; Freire and Meneghini, 2010). Moreover, as pointed out by Jauvtis and Williamson (2003, 2004) in the case of small mass ratio parameter, there is a new branch defined as super-upper branch, characterized by a vortex pattern in which two triplets of vortex are shed in each cycle of oscillation ($2T$ pattern).

Despite the numerous investigations regarding the flow around a non-yawed cylinder, the problem of a yawed cylinder placed in a free stream has received much less attention. Aiming at studying this kind of flow, the most common approach is the Independence Principle (IP). The IP states that the flow characteristics depend only on the component of the free stream velocity normal to the cylinder axis. Herein, the yaw angle θ is defined by the cylinder axis and the direction orthogonal to the free stream, as sketched in Fig. 1(a).

Theoretical investigations presented in Sears (1948) and Marshall (2003) stress that the IP is a bidimensional approach, i.e., valid for a cylinder of infinite length. In this way, there are investigations aimed to check the validity of the IP. Wind tunnel experiments with a tensioned string described in Hanson (1966) stressed that the Strouhal number curve is well

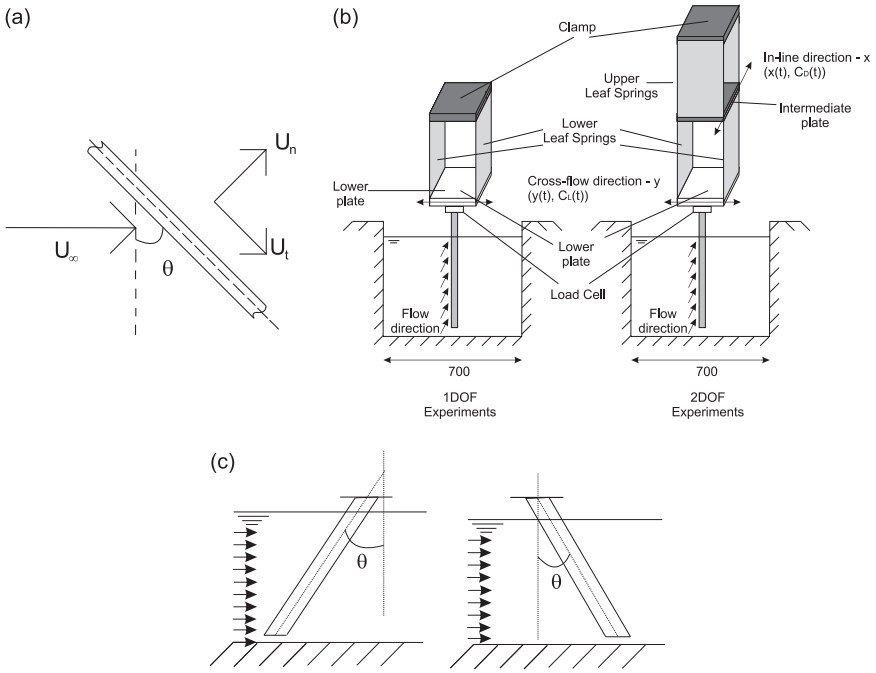

Fig. 1. Schematic representations. (a) Flow around a yawed cylinder, (b) experimental setup, (c) upstream orientation ($\theta < 0$) and (d) downstream orientation ($\theta > 0$).

collapsed by using the IP for values of θ up to 68°. In a similar investigation, van Atta (1968) found that the IP remains valid for yaw angles up to $\theta \approx 35°$.

The experimental investigation described in Ramberg (1983) approached some aspects regarding the characteristics of the flow around a fixed and yawed cylinder. The vortex shedding angle is very sensitive to the end conditions, and by manipulating the end plate angles, the wake is kept parallel to the cylinder axis. Additionally, the paper stressed that the validity of the IP is intrinsically related to the parallel vortex shedding. The flow characteristics dependence on the end conditions, especially the upstream end, were also investigated by Hayashi and Kawamura (1995), Thakur et al. (2004), Matsuzaki et al. (2004) and Hogan and Hall (2010, 2011). Experiments described in Shirakashi et al. (1986) pointed out that the presence of end-plates may remove the secondary (or axial) flow.

The experimental investigation presented in Snarski (2004) pointed out the existence of three distinct flow regimes depending on the yaw angle. For yaw angles ranging from $\theta = 0°$ (non-yawed cylinder) to $\theta \approx 37°$, the flow regime is the classical vortex shedding pattern. In the range $37° < \theta < 68°$, the Strouhal vortex shedding is replaced by a regime in which attached trailing vortexes are observable, in agreement with the previous results of flow visualization described in Thomson and Morrison (1971) and Ramberg (1983). Finally, for yaw angles larger than 78°, an axial boundary layer is observed.

The numerical investigations are also employed as a complementary approach to the experimental studies. For example, the papers by Lucor and Karniadakis (2003) and Zhao et al. (2009) investigated the wake characteristics on the flow around a fixed and yawed cylinder. Jordan (2010) studied the transition to turbulence inside the free shear layers.

Another aspect regarding the flow around the yawed cylinder that may be emphasized is the broadening of the spectral distribution with the increase of θ, as pointed out by Zhou et al. (2009) and Wang et al. (2011).

Regarding the self-excited oscillations of a yawed cylinder, the experimental investigations carried out by employing both a cantilevered cylinder (King, 1977) and a rigid cylinder elastically mounted on a one degree-of-freedom support (Franzini et al., 2009), showed that the IP very well collapses the reduced velocities in which the lock-in is observed, despite a slight decrease in the maximum amplitude. Experiments in a wind tunnel presented by Nakagawa et al. (1998) also investigated the VIV on yawed cylinders with one degree of freedom, but at a much higher mass ratio parameter than the one presented herein. Also for the one degree-of-freedom system, the experimental investigation with yaw angle $\theta = 65°$ described in Jain and Modarres-Sadeghi (2012) pointed out a second lock-in region.

The present paper further investigates VIV on rigid yawed cylinders, for both upstream and downstream orientations and concerns a more detailed discussion of the results presented in Franzini et al. (2012b). Response amplitudes and frequencies, hydrodynamic force coefficients and also the phase shift between force and displacement were evaluated for system constrained to oscillate in one and two degrees of freedom (1-dof and 2-dof respectively).

2. Experimental arrangement and analysis methodology

The experiments were carried out at the recirculating water channel facility at NDF, University of São Paulo. The test section has dimensions 0.70 m × 0.70 m × 7.5 m and can operate with low level of turbulence (≈2%) in free stream velocities up to $U_\infty = 0.40$ m/s. The displacements were obtained through laser sensors LEUZE model ODSL 8/V4 and the forces were measured by an ATI model Mini40 load cell with a resolution of 1/200 N. At the centerline, Assi et al. (2005) found a maximum variation of 5% for the mean value of free stream velocity measured by the flow sensor when compared to the data obtained by using a hot-wire anemometer. The typical uncertainty in the force coefficients was evaluated about 13% by using the procedure described, for example, in Moffat (1988).

A leaf-spring elastic base was employed for both 1-dof and 2-dof experiments (see Fig. 1(b)), similar to the support employed in the 1-dof VIV experimental investigations described by Assi et al. (2006). The apparatus here employed was designed by using a genetic algorithm and a Finite Element Method in order to optimize its parameters for running at the NDF experimental facility. The cylinders were made of aluminium with external diameter $D = 44.4$ mm.

Five yaw angles were tested, namely $\theta = 0°$, 10°, 20, 30° and 45°, where $\theta = 0°$ is the non-yawed case. The cylinder axis remains at the same plane of the free stream velocity. The experiments were carried out for both upstream ($\theta < 0$) and downstream orientations ($\theta > 0$). Fig. 1(c) and (d) presents schematic representation of these orientations. Notice that the upper end of the cylinder pierces the free surface, while its lower end is close to the bottom of the water channel.

For each angle of inclination, the model presented its lower edge parallel to the bottom of the channel. The gap between them was less than $0.5D$. All the experiments were carried out with mass ratio parameter $m^* = 2.6$ and very low structural damping $\zeta_s = c/2\sqrt{km_s} \approx 0.1\%$. The aspect ratio L/D (L is the wet length) was kept constant $L/D \approx 13$ for all the conditions tested by changing the water level according to the yaw angle. The range of the Reynolds number corrected by using the IP was $3 \times 10^3 < \mathrm{Re_n} < 1.5 \times 10^4$. All the data were acquired along 180 s of steady state and with sample frequency $f_{sp} = 100$ Hz.

The oscillation amplitudes were calculated by taking the average of the 10% highest peaks recorded in the time history of displacement $y^*(t) = y(t)/D$ or $x^*(t) = x(t)/D$. This procedure was also adopted by Hover et al. (1997). The frequencies of oscillation, f_{dx} or f_{dy}, refer to the peak in the Power Spectrum Density (PSD) plot. Non-dimensional frequencies of oscillation are defined as $f^*_{dx} = f_{dx}/f_N$ and $f^*_{dy} = f_{dy}/f_N$.

The hydrodynamic forces were normalized by employing the IP; thus, only the component of the free stream velocity normal to the cylinder axis $U_n = U_\infty \cos\theta$ is considered for evaluating the drag and lift coefficients, given respectively by the

following equations:

$$C_{D,n}(t) = \frac{2F_D}{\rho U_n^2 DL} = \frac{2F_D}{\rho U_\infty^2 \cos^2\theta DL}, \tag{1}$$

$$C_{L,n}(t) = \frac{2F_L}{\rho U_n^2 DL} = \frac{2F_L}{\rho U_\infty^2 \cos^2\theta DL}. \tag{2}$$

The reduced velocity $V_{R,n} = U_n/f_N D = U_\infty \cos\theta/f_N D$ was evaluated by considering the validity of the IP and the natural frequency in still water f_N. Throughout the experiments described herein, the free stream velocities range $0.06 < U_\infty < 0.4$ m/s. For the 1-dof experiments the natural frequency is $f_N \approx 0.63$ Hz, independent of the yaw angle. In the 2-dof investigation, the natural frequency lies in the interval $0.69 < f_N < 0.72$ Hz.

The time series of phase shift between force and displacement in the in-line or cross-flow directions (ϕ_x and ϕ_y respectively) was evaluated by using the Hilbert Transform $\mathbf{H}(\cdot)$. F and d being the time series of force and displacement in a given direction, the Hilbert Transform gives the instantaneous amplitude and phase, as follows:

$$\begin{aligned} \mathbf{H}(d) &= a_F(t)e^{j\phi_F(t)}, \\ \mathbf{H}(F) &= a_d(t)e^{j\phi_d(t)}. \end{aligned} \tag{3}$$

Thus, the time series of phase shift between force and displacement will be given simply by $\phi(t) = \phi_F(t) - \phi_d(t)$. It is worth mentioning that the instantaneous phase shift between in-line and cross-flow displacements in a flexible cylinder subjected to VIV was also investigated by Huera-Huarte and Bearman (2009). In this cited paper, the authors were interested in defining the synchronization between the displacements in these directions. In the present investigation, the focus is the synchronization between force and displacement. It can also be emphasized that, for a 1-dof system, Khalak and Williamson (1999) also evaluated the instantaneous phase shift by using the Hilbert Transform and discussed the mode transition from the upper branch to the lower branch.

3. Results and discussion

The present section is divided into four subsections. Sections 3.1 and 3.2 respectively present the results and discussion for the yawed cylinders subjected to 1-dof and 2-dof VIV phenomena. Section 3.3 focuses on the PIV flow measurements for both 1-dof and 2-dof experiments with yaw angles $\theta = 0^\circ$ and $\theta = -45^\circ$. Finally, the last subsection discusses the differences observed between the results for upstream and downstream orientations.

3.1. 1-dof results

The results of non-dimensional oscillation amplitude and frequency are shown in Fig. 2. A first aspect that can be noted is the marked difference between the results for upstream and downstream orientations. Another clearly visible aspect is the fact that the use of the IP in the evaluation of the reduced velocity very well corrects the lock-in range, in agreement with the previous results described in Franzini et al. (2009).

For the upstream case, despite a slight decrease in the maximum oscillation amplitude for $\theta = -30^\circ$ and $\theta = -45^\circ$, there is good agreement between the results of amplitude Fig. 2(a) and frequency (Fig. 2(c)) for all the angles tested in the range of reduced velocities named initial branch ($2 < V_{R,n} < 4$) and upper branch ($4 < V_{R,n} < 6.5$). Also for $\theta = -30^\circ$ and $\theta = -45^\circ$, as the reduced velocity increases, the amplitude decreases more slowly than in the other angles, and the lower branch is not observed.

Considering the downstream cases, a decrease in the response amplitude is observed for angles larger than $\theta = \pm 20^\circ$. The maximum response amplitude reaches $A_y^* \approx 0.9$ in the case $\theta = +20^\circ$ and $A_y^* \approx 0.6$ for $\theta = +30^\circ$ and $\theta = +45^\circ$. Notice that the decrease in the response amplitude is more pronounced than that observed in the results obtained from the upstream orientation. Focusing on the analysis of the non-dimensional frequencies, shown in Fig. 2(d), the f_{dy}^* results for the $\theta = +45^\circ$ cases are slightly higher than those from the experiments with smaller yaw angles.

Fig. 3 illustrates the differences between upstream and downstream time series of non-dimensional displacement and the related PSD at reduced velocity $V_{R,n} \approx 5.9$. Notice that, for the upstream orientation case, the PSD plot presents a narrower band than the spectrum obtained from the downstream orientation case.

The results for the mean drag coefficient, as well as the r.m.s. lift coefficient, are presented in Fig. 4. As stressed, for example, in the papers by Sarpkaya (1995), Khalak and Williamson (1999) and Franzini et al. (2012a), the presence of the lock-in (and consequently, cylinder motion) is responsible for the increase in the force coefficients. As the IP well collapses the range of reduced velocities in which the lock-in occurs, it represents a useful approach aiming at correcting the interval of reduced velocity where the higher forces coefficients are observed.

Besides the correction of the range of reduced velocities, the IP very well collapses the values of the r.m.s. lift coefficient for both upstream and downstream orientations cases, as can be found in Fig. 4(a) and (b), respectively. This result is in agreement with that presented in Franzini et al. (2009), in spite of the differences in the experimental setups.

The use of the IP for the evaluation of the mean drag coefficient deserves a more detailed discussion. For both the orientations, the values of $\overline{C}_{D,n}$ decrease with the increase in the yaw angle. Notice that, for both the orientations tested, the

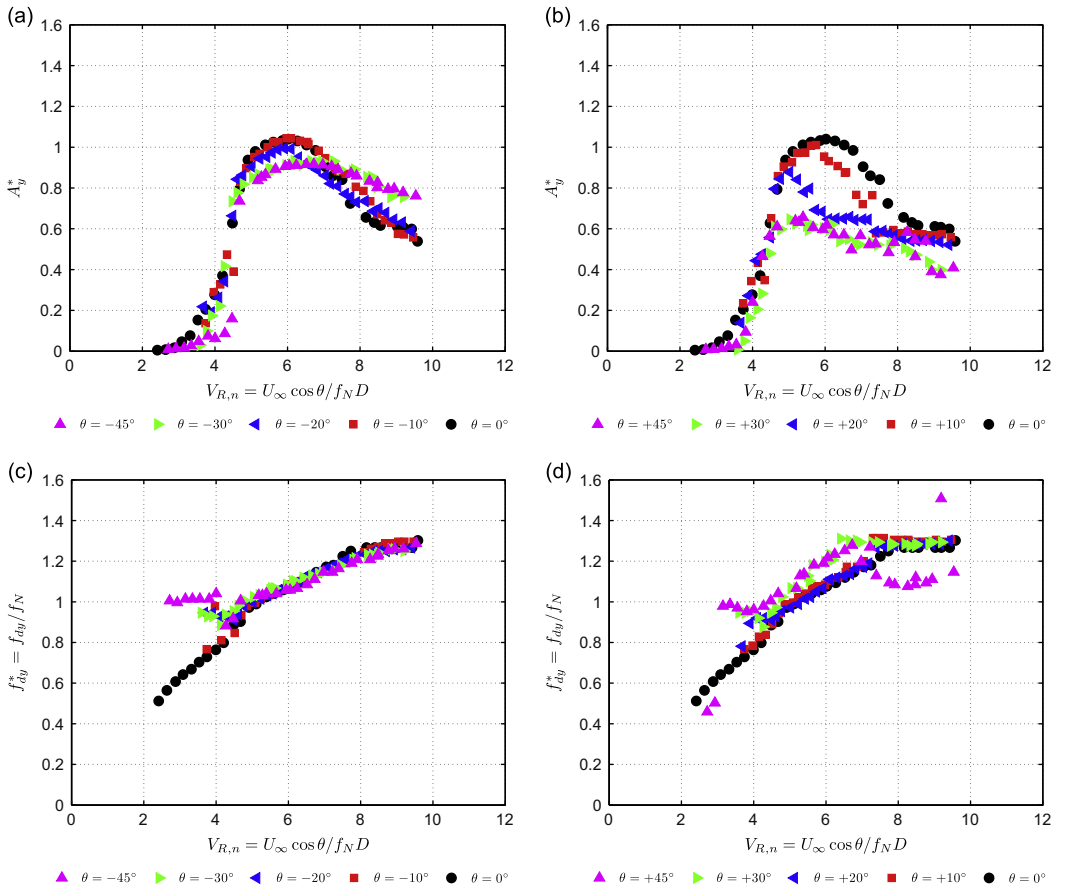

Fig. 2. Non-dimensional oscillation amplitude and frequency. 1-dof experiments. (a) Amplitude – upstream, (b) amplitude – downstream, (c) frequency – upstream and (d) erequency – downstream.

asymptotic result from a fixed cylinder $\overline{C}_{D,n}\approx 1$ is recovered in the absence of lock-in ($V_{R,n} < 4$ and $V_{R,n} > 10$). The presence of lock-in and, consequently, large oscillation amplitudes (order of 1D), increase both the mean drag coefficient and the r.m.s. lift coefficient, as already stressed by Sarpkaya (1995) and Khalak and Williamson (1999). Owing to the differences in the oscillation amplitudes obtained for the upstream and downstream orientations, the mean drag coefficient also depends on the orientation.

Aiming at better understanding the relationship between the mean drag coefficient and the oscillation amplitude, Fig. 5 is plotted. Considering the upstream experiments, shown in Fig. 5(a), function $\overline{C}_{D,n}(A_y^*)$ follows the same trend for all the yaw angles tested. This result indicates that the upward trend in the $\overline{C}_{D,n}$ with the oscillation amplitude is independent of the yaw angle. On the other hand, the results for the downstream case (Fig. 5(b)) show that this fact is not valid for the latter orientation.

The last aspect investigated for the 1-dof experiments is the phase shift between the lift force and the cylinder displacement. First, the analysis is carried out at reduced velocity $V_{R,n}\approx 5.9$, corresponding to the peak of oscillation amplitude for the non-yawed cylinder. Fig. 6 presents the time series of phase shift $\phi_y(t)$ and the corresponding histogram for the cases with $\theta = 0°$, $\theta = \pm 30°$ and $\theta = \pm 45°$.

The time series $\phi_y(t)$ corresponding to the non-yawed case is shown in Fig. 6(a). The highest number of occurrences at the histogram indicates that the phase shift is lower than 20°, although some jumps to 180–200° interval can also be observed. Within the scope of linear systems with very low damping, the phase shift between force and displacement is null before the resonance, with a jump of 180° after it. The jumps observed in the time series are associated to the transition between the upper branch and the lower branch, in good agreement with the previous findings described in Khalak and Williamson (1999).

Before the analysis of the yawed cylinders, a more general definition should be made. In the book by Pikovsky et al. (2001), synchronization occurs if the phase shift between two signals of the same dominant frequency remains constant along the time. Herein, we are interested in studying the synchronization between hydrodynamic forces and displacement. For the 1-dof system, $\phi_y(t)$ is the time history of phase shift between the lift force and the cross-flow displacement. Keeping this aspect in mind, the results for the upstream orientation cases, shown in Fig. 6(b) and (d), the phase shift is almost constant all along the time span, as in Fig. 6.

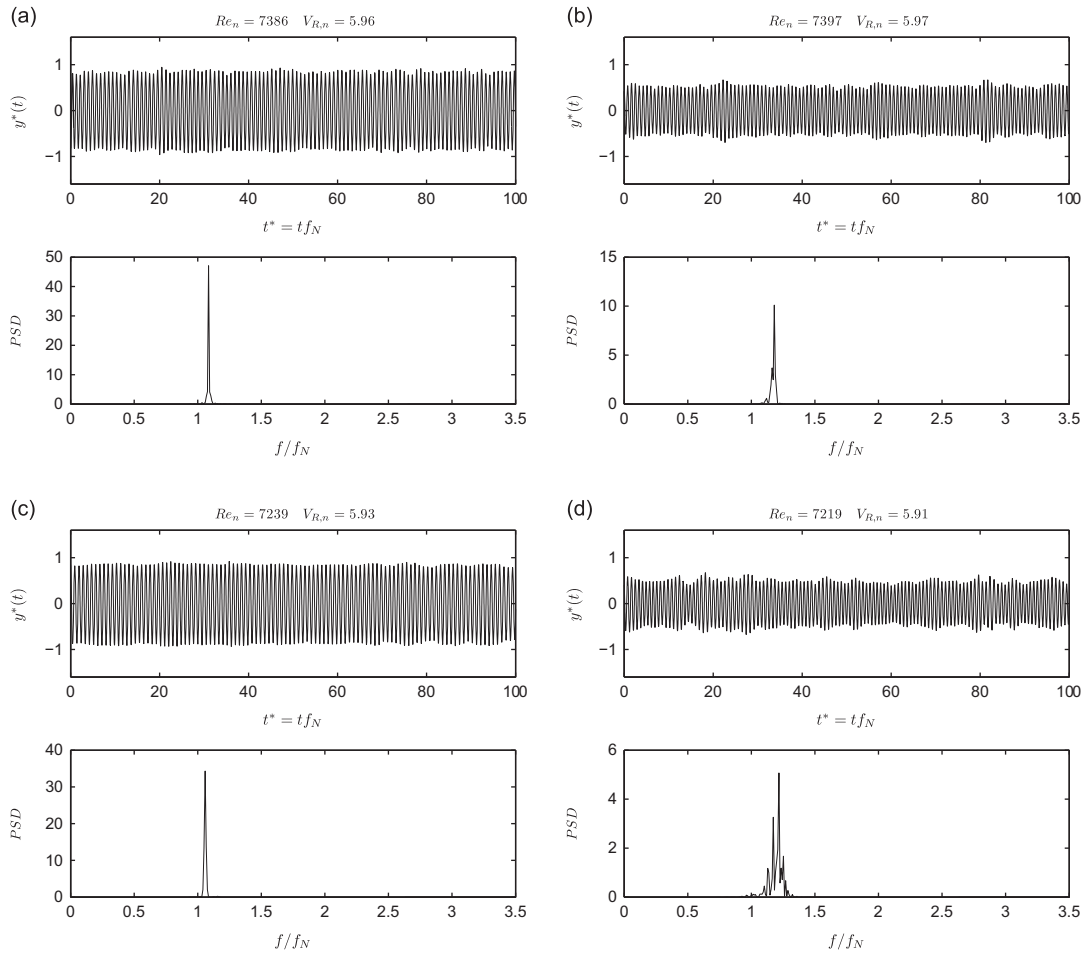

Fig. 3. Time series of displacement at $V_{R,n}$≈59 for $\theta = \pm 30^\circ$ and $\theta = \pm 45^\circ$. 1-dof experiments. (a) $\theta = -30^\circ$, (b) $\theta = +30^\circ$, (c) $\theta = -45^\circ$ and (d) $\theta = +45^\circ$.

On the other hand, the time series $\phi_y(t)$ for the downstream orientation experiments (see Fig. 6(c) and (e)) is much sparser than those for the upstream case. Thus, it can be concluded that the upstream orientation experiments present a well-defined synchronization between the force and the cylinder displacement than that observed in the downstream case. This can explain the higher oscillation amplitudes and narrower PSD plot observed in the upstream experiments.

3.2. 2-dof results

The oscillation amplitudes and frequencies for both the cross-flow and in-line directions are presented in Figs. 7 and 8 respectively. As observed for the 1-dof experiments and discussed in Section 3.1, the IP greatly corrects the range of reduced velocities in which the highest amplitudes are observed.

In the range $2 < V_{R,n} < 4$, in-line oscillations with amplitudes A_x^*≈0.1 are observed for yaw angles up to $\theta = \pm 20^\circ$. The oscillation frequency for these experiments obeys the relation f_{dx}≈$2f_{dy}$. These results are in good agreement with the previous investigation carried out with a non-yawed cylinder and presented in the paper by Jauvtis and Williamson (2004). Still considering the same range of reduced velocities, the ratio f_{dx}/f_{dy}≈2 is not observed for the cases with $\theta = \pm 30^\circ$ and $\theta = \pm 45^\circ$, leading to a marked decrease in the in-line oscillation amplitude.

As observed for the in-line resonance range ($2 < V_{R,n} < 4$), at the interval $4 < V_{R,n} < 7.5$ (corresponding to the super-upper branch of a non-yawed cylinder, in the nomenclature adopted in Jauvtis and Williamson, 2004) the oscillation amplitude plot agrees very well for yaw angles up to 20° in both orientations. Also, notice that the in-line oscillation frequency is twice the cross-flow one, as can be seen in Fig. 8(a) and (b).

Following the trend observed in the in-line resonance range, there is a decrease in the oscillation amplitudes in both directions for the experiments with $\theta = \pm 30^\circ$ and $\theta = \pm 45^\circ$. Similar to the results for the 1-dof investigations in the downstream orientation, the cross-flow frequencies of oscillation Fig. 8(d) for the cases with $\theta > \pm 20^\circ$ are higher than those for the $\theta = 0^\circ$. Converse to the 1-dof results for the largest yaw angles, the cross-flow frequency of oscillation, presented in Fig. 8(c), indicates a slight deviation from the results obtained with the non-yawed cylinder.

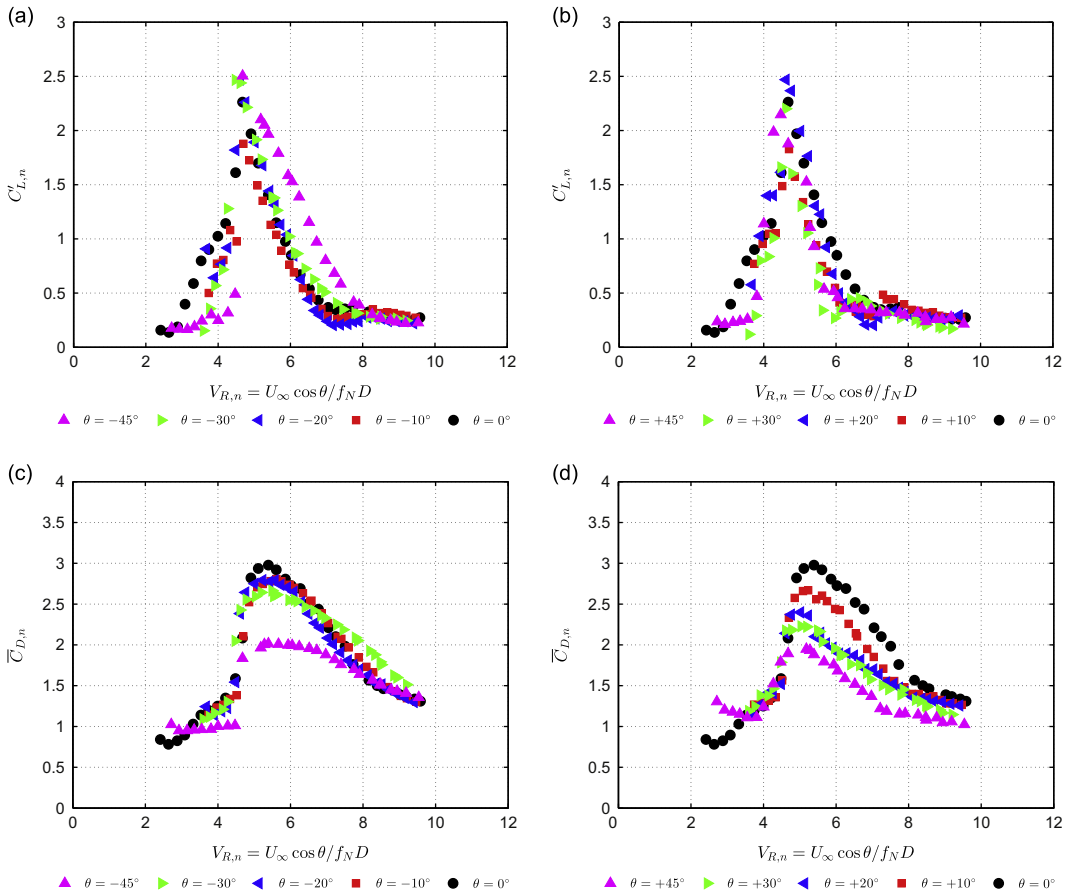

Fig. 4. Force coefficients. 1-dof experiments. (a) $C'_{L,n}$ – upstream, (b) $C'_{L,n}$ – downstream, (c) $\overline{C}_{D,n}$ – upstream and (d) $\overline{C}_{D,n}$ – downstream.

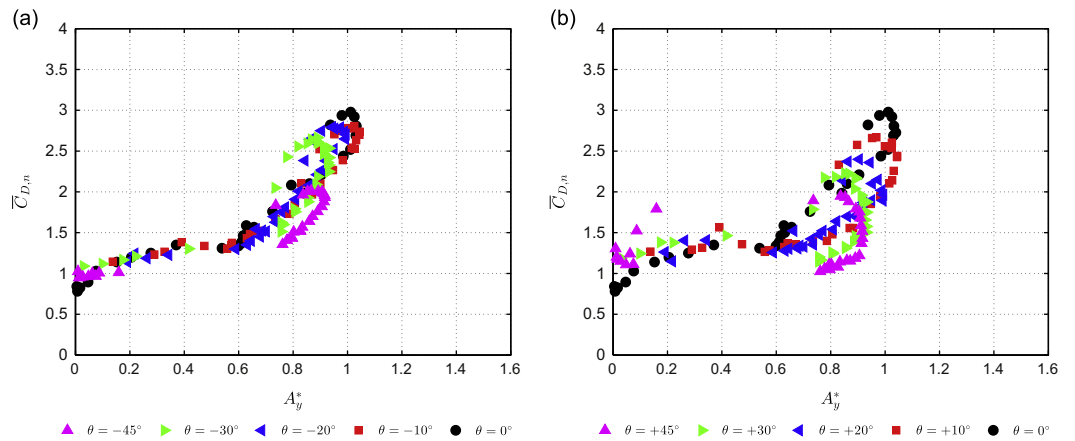

Fig. 5. Mean drag coefficient dependence on the oscillation amplitude. 1-dof experiments. (a) Upstream and (b) downstream.

The analysis of the time histories of displacement can help to better understand the differences between upstream and downstream results. Figs. 9, 10 and 11 present, respectively, the time series for $\theta = 0°$, $\theta = \pm 30°$ and $\theta = \pm 45°$ at $V_{R,n} = 6.2$. For the non-yawed case, both spectra are narrow banded and the $f_{dx}/f_{dy} = 2$ relation is observed, despite a visible $f/f_N = f_{dy}$ component in the in-line spectrum, but with much less energy.

Changing the yaw angle to $\theta = -30°$, the in-line and cross-flow spectral bands are broader than those observed in the $\theta = 0°$ case, but the most relevant difference is related to the fact that $f_{dx} \approx f_{dy}$, despite the cross-flow oscillation amplitude

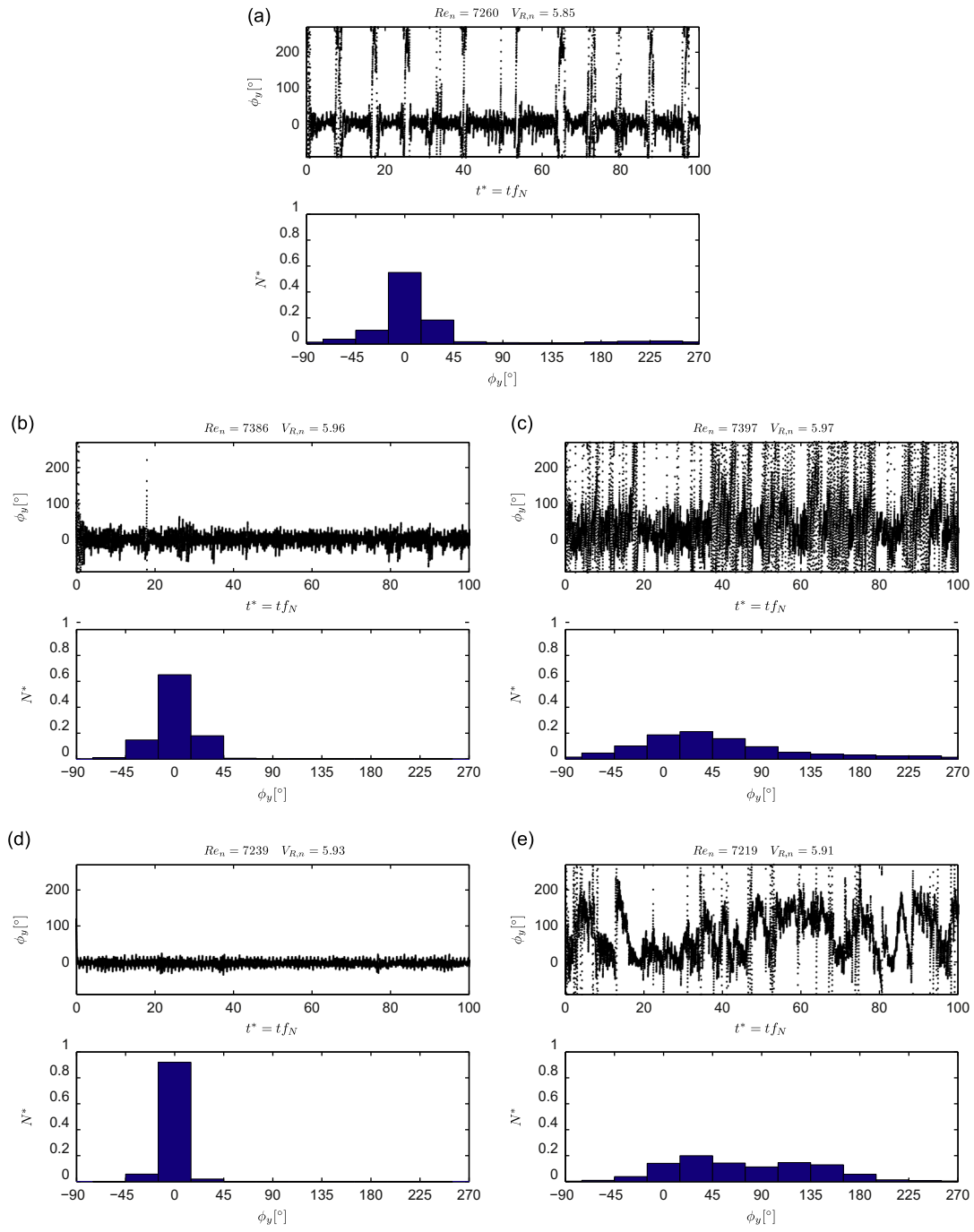

Fig. 6. Phase shift between lift force and displacement ϕ_y at $V_{R,n}$≈5.9. 1-dof experiments. (a) $\theta = 0^\circ$, (b) $\theta = -30^\circ$, (c) $\theta = +30^\circ$, (d) $\theta = -45^\circ$ and (e) $\theta = +45^\circ$.

being close to the non-yawed case. On the other hand, considering the downstream orientation experiments $\theta = +30^\circ$ (Fig. 10(c) and (d)), the time series and related PSD plots present good agreement with the non-yawed results.

A new increase to yaw angles $\theta = \pm 45^\circ$ reveals a marked difference of the time histories and its spectral content if compared to the $\theta = 0^\circ$ case, as can be seen in Fig. 11. The ratio f_{dx}/f_{dy}≈1 is observed for both orientations, the spectral bands for the upstream condition being narrower than those for the downstream case.

Aiming at a better visualization of the effects of the yaw angle on the cylinder motion at 2-dof, Figs. 12 and 13 present the trajectories at the (x^*, y^*) plane for reduced velocities up to $V_{R,n}$≈8 and all the conditions tested. At $V_{R,n} = 3.2$, there is no distinction between the trajectories for the non-yawed cylinder or for the cylinder yawed in $\theta = \pm 10^\circ$. Considering

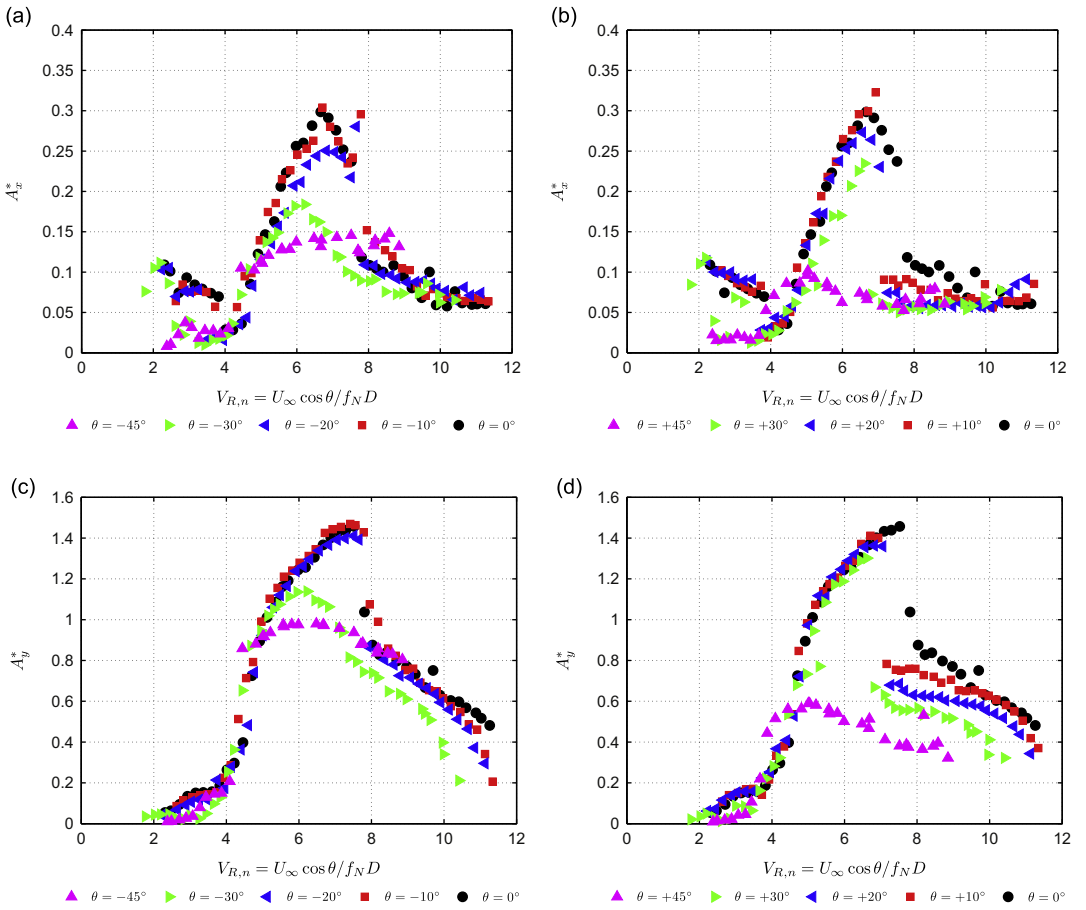

Fig. 7. Non-dimensional oscillation amplitude. 2-dof experiments. (a) In-line amplitude A_x^* – upstream, (b) in-line amplitude A_x^* – downstream, (c) cross-flow amplitude A_y^* – upstream and (d) cross-flow amplitude A_y^* – downstream.

$\theta = \pm 20°$, the oscillation amplitudes are slightly lower than those for the case with $\theta = 0°$, but the less defined *8-shape* trajectory can be an indicative of a less defined synchronization process. The synchronization for the 2-dof experiments will be better discussed in this section.

At $V_{R,n} = 6.2$, the *8-shape* trajectory for $\theta = 0°$ and $\theta = \pm 10°$ arises from the fact that $f_{dx} \approx 2f_{dy}$. By increasing the yaw angle, the trajectories are verified to become less defined and the oscillation amplitudes are decreased. Especially at yaw angles larger than 30°, the classical *8-shape* is no longer observed because of the broadening of the spectral band and, mainly, because $f_{dx} \approx f_{dy}$. The analysis of this trajectory suggests modifications in the wake characteristics for yaw angles $\theta = -45°$. This aspect will be better discussed in Section 3.3.

At $V_{R,n} = 7.5$, the transition from the super-upper branch to the lower branch occurs for the non-yawed cylinder, with the corresponding *C-shape* trajectory. Especially in the downstream orientation, there are marked differences among the trajectories for $\theta = 0°$ and the yawed cases. Finally, at reduced velocity $V_{R,n} = 8$, the in-line oscillation amplitudes are negligible for all the yaw conditions tested.

After the discussion regarding the time histories of displacement, the force coefficient plots will be discussed. Fig. 14 presents the mean drag and r.m.s. lift force coefficients for the 2-dof experiments. Similar to that observed in the 1-dof discussion, the IP corrects the interval of reduced velocities in which the higher forces are observed because the lock-in range is corrected very well.

The force coefficient plots for yaw angles of $\theta = \pm 10°$ and $\theta = \pm 20°$ are in good agreement with those obtained from the non-yawed for the whole range of velocities. For these yaw angles and in the in-line resonance range, one can notice that both the mean drag and the r.m.s. lift force coefficients present a marked amplification of their values, if compared with the results for a fixed cylinder, despite the small in-line oscillation amplitudes. Clearly, the force amplification in the in-line resonance range of reduced velocities is not observed for experiments with larger yaw angles, which present the asymptotic result well known for a fixed and non-yawed cylinder $\overline{C}_{D,n} \approx 1$. More details regarding the force amplification due to the synchronization for the non-yawed cylinders can be found in Jauvtis and Williamson (2004) and Franzini et al. (2012a).

In the range of reduced velocities $4 < V_{R,n} < 7.5$ and for the yaw angles $\theta = \pm 30°$ and $\theta = \pm 45°$, a drastic reduction can be noticed in the $C'_{L,n}$ results when compared to those observed at small yaw angles. On the other hand, the mean drag

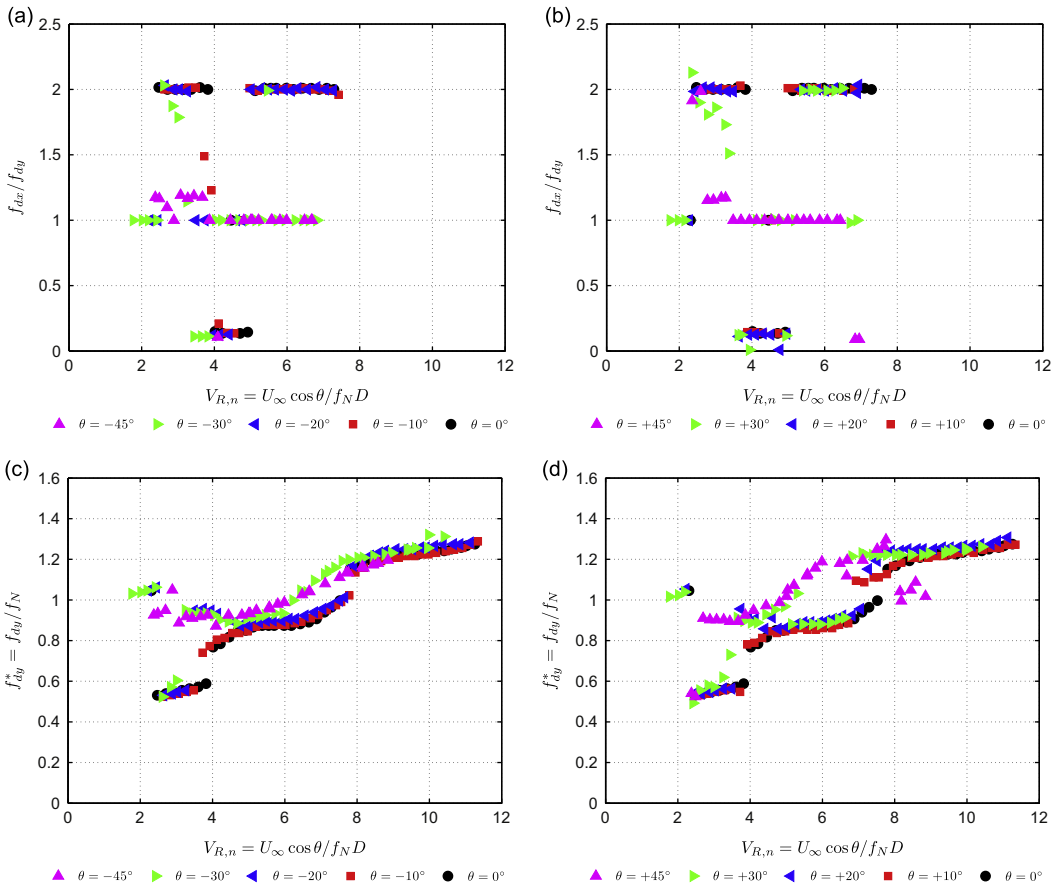

Fig. 8. Non-dimensional oscillation frequency. 2-dof experiments. (a) Ratio f^*_{dx}/f^*_{dy} – upstream, (b) ratio f^*_{dx}/f^*_{dy} – downstream, (c) ratio $f^*_{dy} = f_{dy}/f_N$ – upstream and (d) ratio $f^*_{dy} = f_{dy}/f_N$ – downstream.

coefficient values are comparable to those from the non-yawed case, despite presenting slightly lower values, in agreement with the lower oscillations amplitudes. The analysis of the time series allows a better understanding regarding the differences in amplitude and force coefficient observed for angles larger than 45°.

Fig. 15 presents the time series of lift force coefficient for the cases with $\theta = 0°, \pm 30°, \pm 45°$ at $V_{R,n} \approx 6.2$. In the spectrum obtained from the non-yawed case (see Fig. 15(a)), not only the contribution of the dominant frequency $f/f_N \approx 0.87$ is visible, but also the third subharmonic $f/f_N \approx 2.6$.

The time histories for the cases corresponding to $\theta = \pm 30°$ are shown in Fig. 10(a) and (c). Besides the marked decrease in the maximum value, the broadening of the spectral content for both the dominant and the third subharmonic frequency can be observed. Considering the time histories obtained from the $\theta = \pm 45°$ (Fig. 15(d) and (e)), the amplitude of $C_{L,n}(t)$ is lower and the bandwidth is larger than those observed in the experiments with the cylinder yawed in $\theta = \pm 30°$.

Similar to the approach employed for the 1-dof results, we can carry out an analysis aiming at identifying the relationship between the mean drag coefficient and the oscillation amplitude. Fig. 16 presents the variation of the mean drag coefficient with the cross-flow oscillation amplitude for the 2-dof results. Considering the upstream results (Fig. 16(a)), the upward trend of $\overline{C}_{D,n}$ with A^*_y being the same for all yaw angles tested, excepting the results for the in-line resonance range ($A^*_y < 0.2$), in which the force amplification is not observed for the conditions corresponding to $\theta = -30°$ and $\theta = -45°$. Notice that this result was also observed for the 1-dof system. Moreover, for the downstream orientation, the upward trend of $\overline{C}_{D,n}(A^*_y)$ observed for $\theta = 0°$ is significantly different from that $\theta = +45°$.

The last set of results concerns the phase shift for the yaw angles $\theta = 0°, \theta = \pm 30°, \theta = \pm 45°$ at reduced velocity $V_{R,n} = 6.2$. In the 2-dof cases, the analysis must focus not only on the phase shift between lift force and cross-flow displacement, but also on that between the oscillatory component of the drag force and the in-line displacement.

The time histories $\phi_x(t)$ and $\phi_y(t)$ for the non-yawed experimental case are presented in Fig. 17. At reduced velocity $V_{R,n} = 6.2$, there is a condition in which the dominant response is that corresponding to the super-upper branch; hence, the in-line resonance is no longer observed and the transition to the lower branch has not occurred. Invoking again the classical

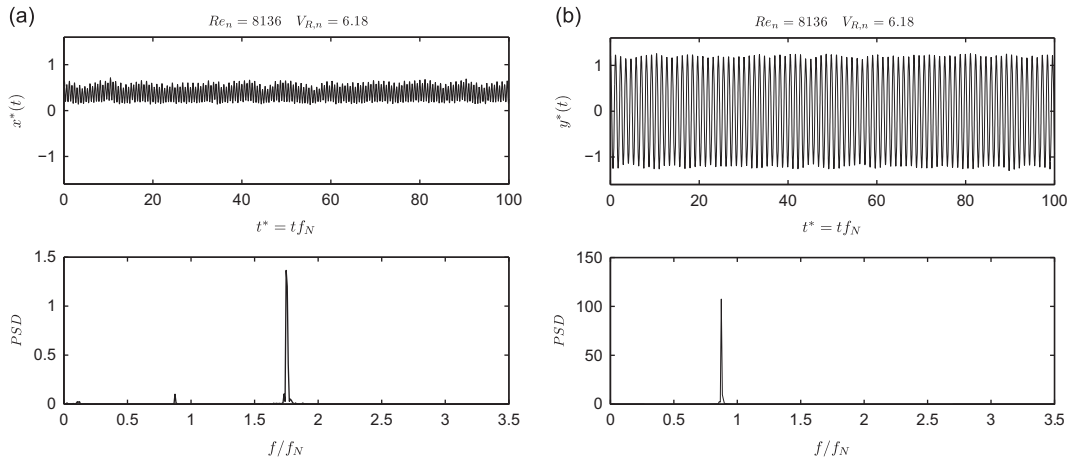

Fig. 9. Time series of displacement at $V_{R,n}$≈6.2 and $\theta = 0^\circ$. 2-dof experiments. (a) $x^*(t)$ and PSD – upstream and (b) $y^*(t)$ and PSD – downstream.

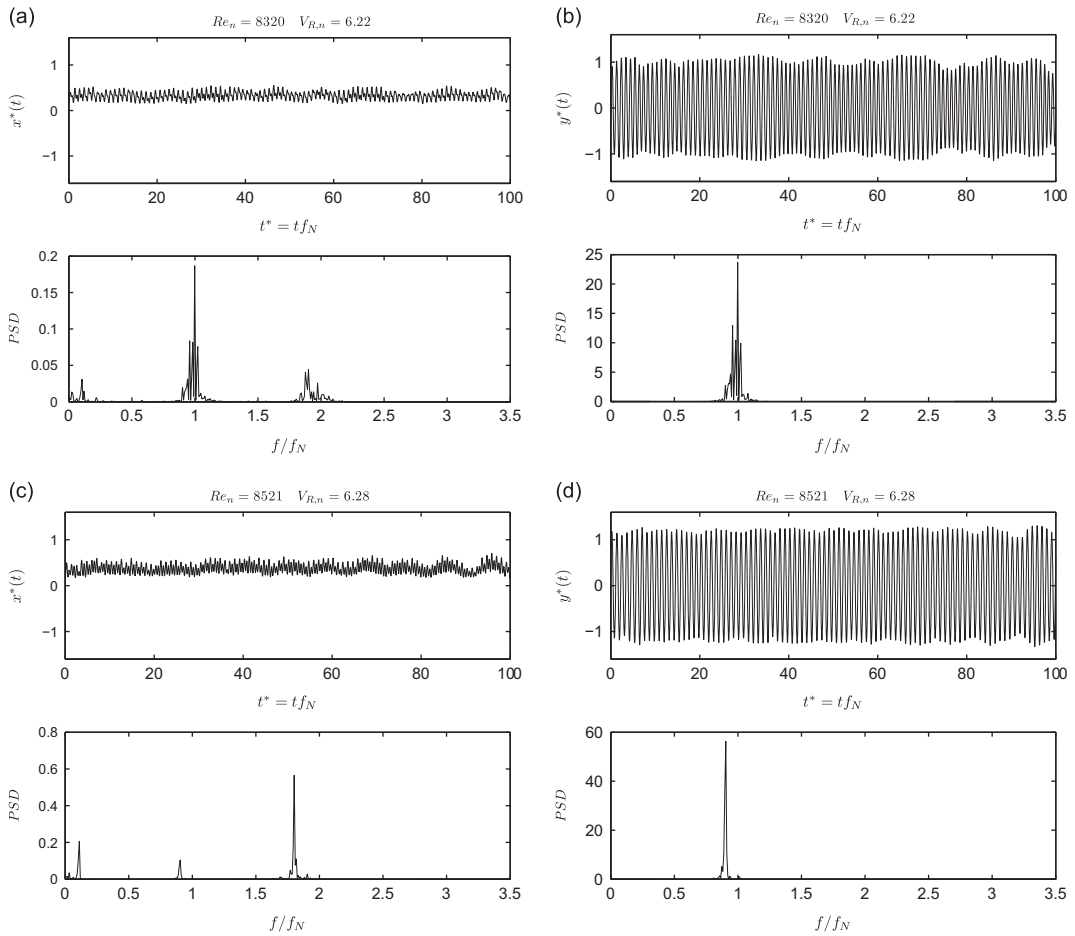

Fig. 10. Time series of displacement at $V_{R,n}$≈6.2 and $\theta = \pm 30^\circ$. 2-dof experiments. (a) $x^*(t)$ and PSD – upstream, (b) $y^*(t)$ and PSD – upstream, (c) $x^*(t)$ and PSD – downstream and (d) $y^*(t)$ and PSD – downstream.

results from the linear dynamics, the phase shifts ϕ_x and ϕ_y are expected to behave similar to that observed in a linear system after and before the resonance, respectively. This assertion is experimentally verified because both the in-line and cross-flow phase shifts present almost no modulation around the characteristic values ϕ_x≈180° and ϕ_y≈0°. According to the definition by Pikovsky et al. (2001), the synchronization process at this condition is very well defined, leading to a very clear

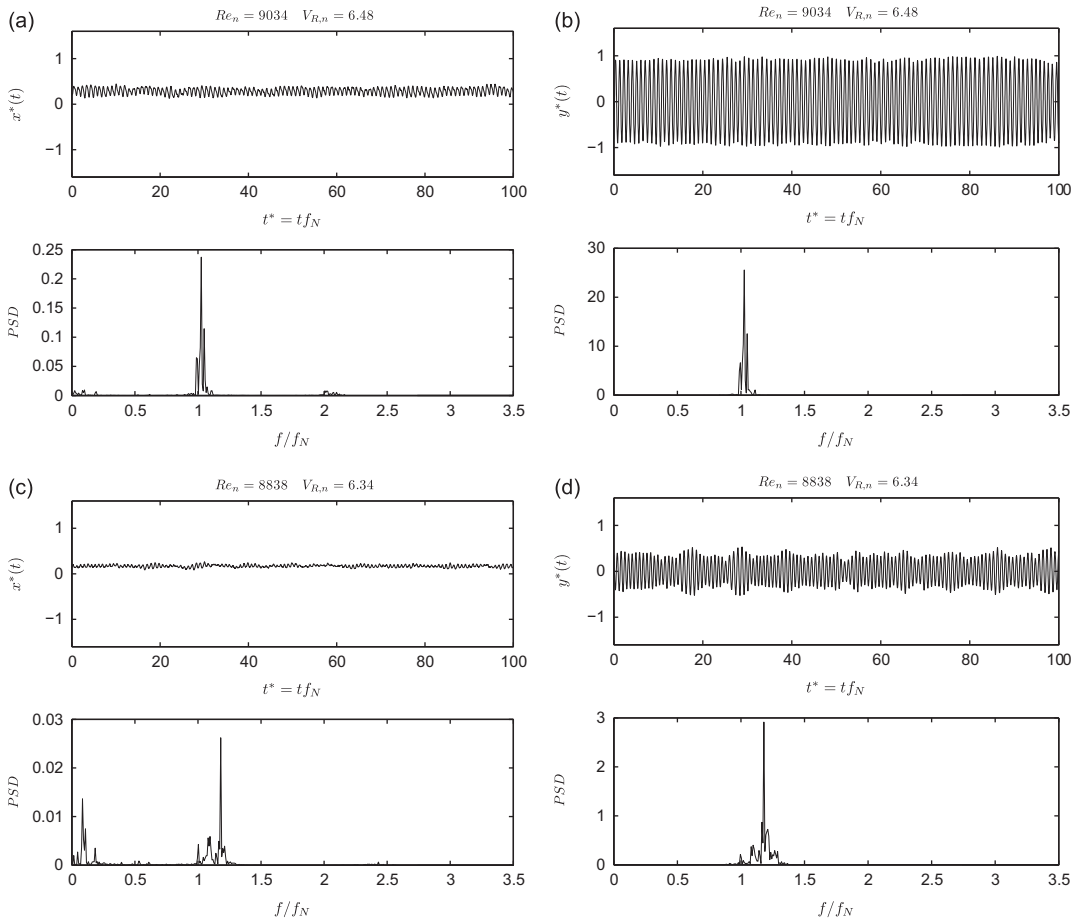

Fig. 11. Time series of displacement at $V_{R,n}$≈6.4 and $\theta = \pm 45^\circ$. 2-dof experiments. (a) $x^*(t)$ and PSD – upstream, (b) $y^*(t)$ and PSD – upstream, (c) $x^*(t)$ and PSD – downstream and (d) $y^*(t)$ and PSD – downstream.

trajectory in the (x^*, y^*) plane, as can be seen in Fig. 12. It is worth mentioning that the phase shift results for the non-yawed cylinder agree with those available in the literature, for example, in Jauvtis and Williamson (2004).

Fig. 18 presents the instantaneous phase shift time histories for the cases in which the cylinder is yawed in $\theta = \pm 30^\circ$. The in-line phase shift $\phi_x(t)$ (Fig. 18(a) and (c)) shows a different behavior from that observed for the non-yawed case. Contrary to the latter case, there are strong modulations observed for both orientations, even though the downstream case is less modulated. In spite of the mean value matching the non-yawed condition, the instantaneous cross-flow phase shift $\phi_y(t)$, shown in Fig. 18(b) and (d), is also more modulated than that observed for the $\theta = 0^\circ$ case.

The phase shifts for the $\theta = \pm 45^\circ$ experiments are shown in Fig. 19. For both orientations, the in-line phase shifts are found to be even more modulated than those observed in the discussion regarding the $\theta = \pm 30^\circ$ results, as can be noted in Fig. 19(a) and (c). The cross-flow phase shift time series, presented in Fig. 19(b) and (d), reveals an interesting aspect. The result for the upstream case indicates a condition close to the cross-flow resonance jump (transition to the lower branch), while the time series for the downstream case is similar to that after the resonance. As found for the non-yawed case, the transition to the lower branch is expected to occur at reduced velocity $V_{R,n}$≈7.5, thus the referred transition is anticipated with the increase in the yaw angle. Moreover, the transition is observed at reduced velocity close to that in which the jump from the upper branch to the lower branch occurs for the 1-dof system.

The progressive distortion of the $3f_{dy}$ subharmonic in the $C_{L,n}(t)$ spectral content, combined with the anticipation of the jump to the lower branch, indicates that the yaw angle and, consequently, the presence of axial flow, seems to change the wake characteristics. The flow measurements described in Section 3.3 confirm this fact.

It is worth mentioning that the experimental results presented in Snarski (2004) with a fixed and yawed cylinder at $\mathrm{Re} = 7.2 \times 10^3,\ 1.35 \times 10^4,\ 2.76 \times 10^4$ show that there is a transition in the flow regime characterized by the Strouhal vortex shedding to another regime characterized by attached trailing vortex at yaw angle θ≈37°. Ramberg (1983) also found this flow regime transition at a similar yaw angle θ≈30°, but for smaller Reynolds numbers ($160 < \mathrm{Re} < 1000$). Thus different flow regimes under the VIV phenomenon at yaw angles larger than 30° are similar to the previous results for a fixed cylinder.

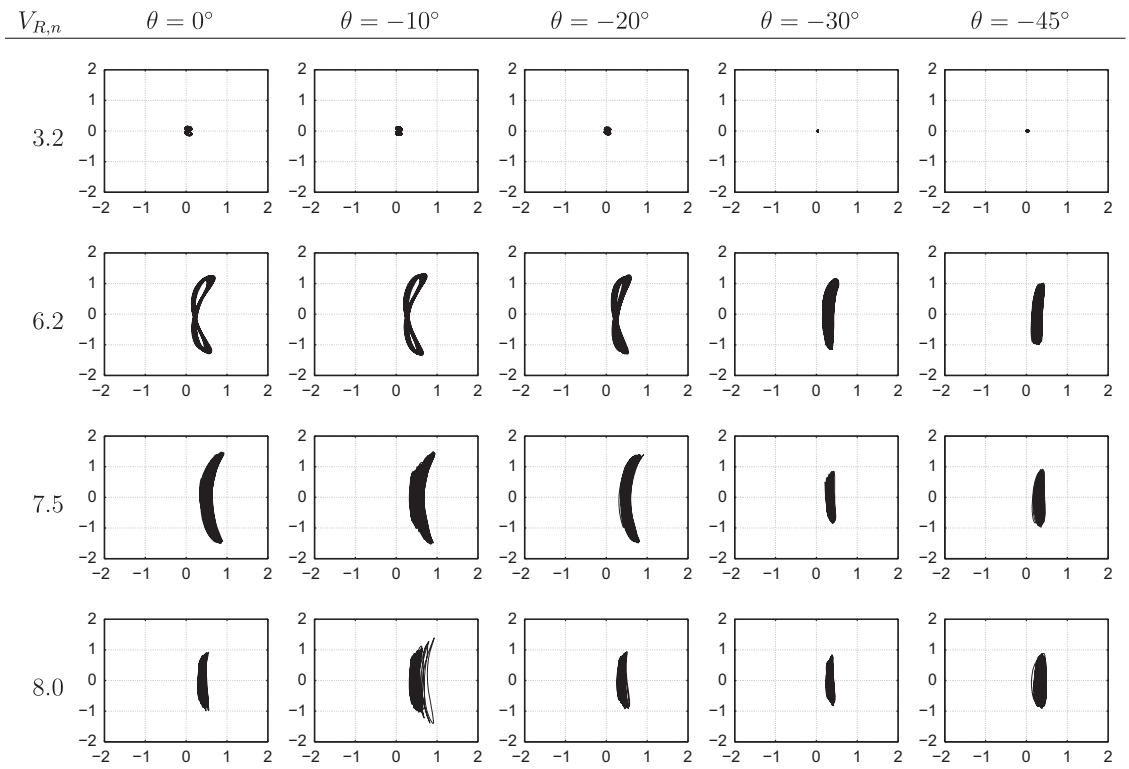

Fig. 12. (x^*,y^*) trajectories – upstream orientation and $3.2 < V_{R,n} < 8.0$.

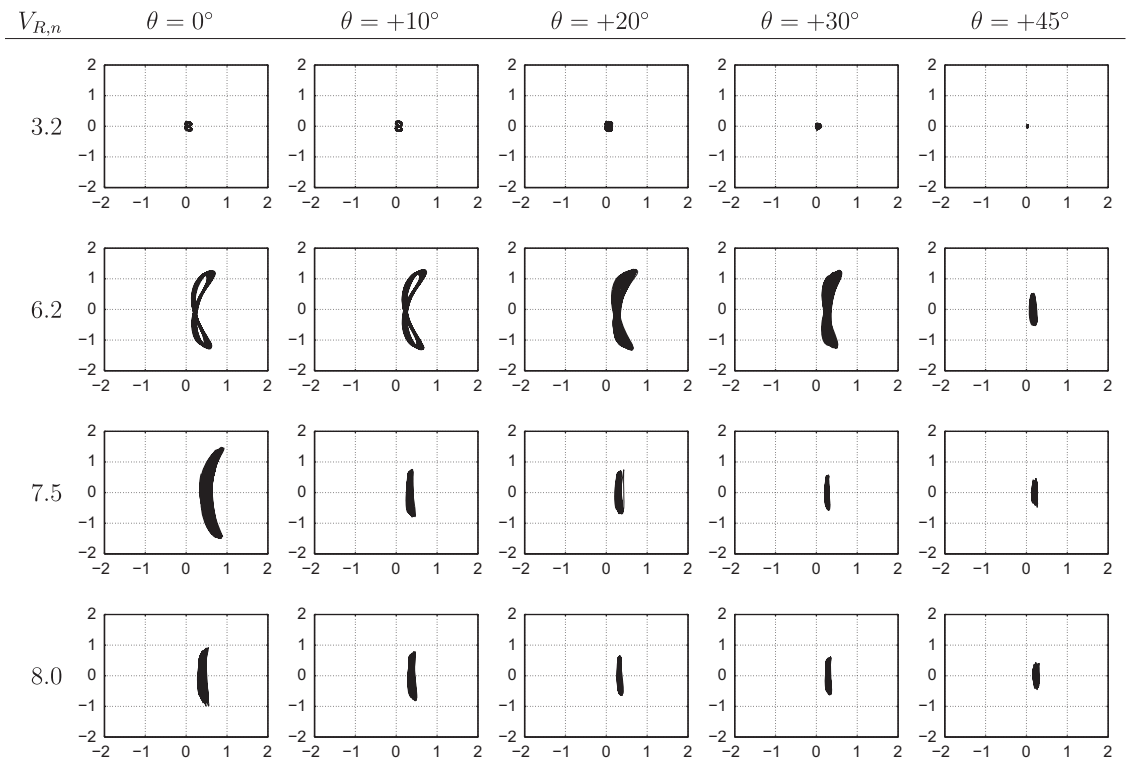

Fig. 13. (x^*,y^*) trajectories – downstream orientation and $3.2 < V_{R,n} < 8.0$.

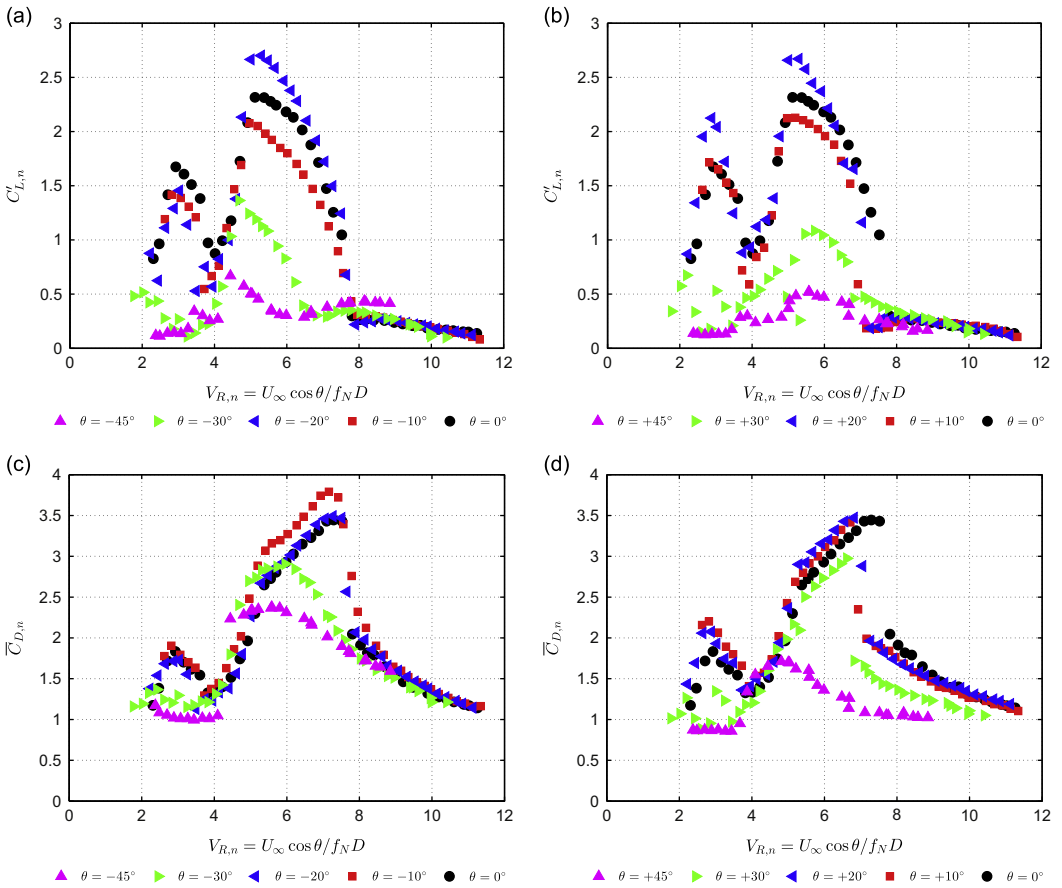

Fig. 14. Force coefficient – 2-dof experiments. (a) $C'_{L,n}$ – upstream, (b) $C'_{L,n}$ – downstream, (c) $\overline{C}_{D,n}$ – upstream and (d) $\overline{C}_{D,n}$ – downstream.

3.3. Flow measurements

For the yaw conditions $\theta = 0^\circ$ and $\theta = -45^\circ$ and at $V_{R,n} \approx 6.2$ ($\mathrm{Re_n} \approx 8 \times 10^3$), 2D flow measurements were carried out using the same particle image velocimetry (PIV) facility described in Korkischko and Meneghini (2011). The optical system was composed of a Nikon lens, model AF Nikkor $f/1.4D$ with focal length 50 mm, an Imager Pro X 2 Megapixel camera and a Quantel (Brilliant Twins) double-cavity pulsed Nd:YAG laser system (532 nm wavelength). The measurements were carried out at a horizontal plane which was $5.5D$ far from the channel floor.

The water was seeded with polyamide particles about 11 μm in diameter and density close to 1030 kg/m^3. As in Korkischko and Meneghini (2011), the vector fields were calculated using the DaVis 7.2 software, employing a two-pass windowing process with decreasing size. The fist step employed a 64×64 pixel interrogation window and the second step concerned a correlation with a 32×32 pixel window. The sample frequency was fixed and equal to 14.8 Hz for all the experiments, allowing obtaining a total number of 345 snapshots. The time lapse between two consecutive laser shots was $\Delta\tau = 5000$ μs for the non-yawed cases and $\Delta\tau = 4500$ μs for the $\theta = -45^\circ$ cases. The time lapses were defined by measuring the flow in the absence of the cylinder. In this condition, the maximum r.m.s. of the flow field is close to 5% of the mean value. The image domains covered approximately 3 diameters in the in-line direction and 4 diameters in the cross-flow direction.

The flow fields concern an analysis of post-processed data using the phase-average technique. The first step of this technique consists in choosing a desired phase (snapshot) within one cycle of cylinders displacement. Herein, the desired phase was chosen as that in which the cylinder is at the maximum cross-flow displacement. Using the sample frequency of the PIV system and the dominant frequency of oscillation, we evaluated the corresponding snapshots in the other cycles. At least 16 cycles of cross-flow displacement were obtained in the PIV measurements. Hence, the fields presented herein consist of the averaged result considering the 16 identified snapshots.

Fig. 20 presents the phase-averaged vorticity fields ω_z obtained by using the PIV system. The flow measurements were carried out for both the one and two degrees of freedom.

Qualitatively, there are differences in the wake characteristics of the non-yawed cases (Fig. 20(a) and (c)) and the $\theta = -45^\circ$ ones (Fig. 20(b) and (d)). For both 1-dof and 2-dof tests at $\theta = -45^\circ$, it can be inferred that the presence of axial flow interferes with the interaction between the free shear layers, as can be seen in the vorticity fields presented in Fig. 20

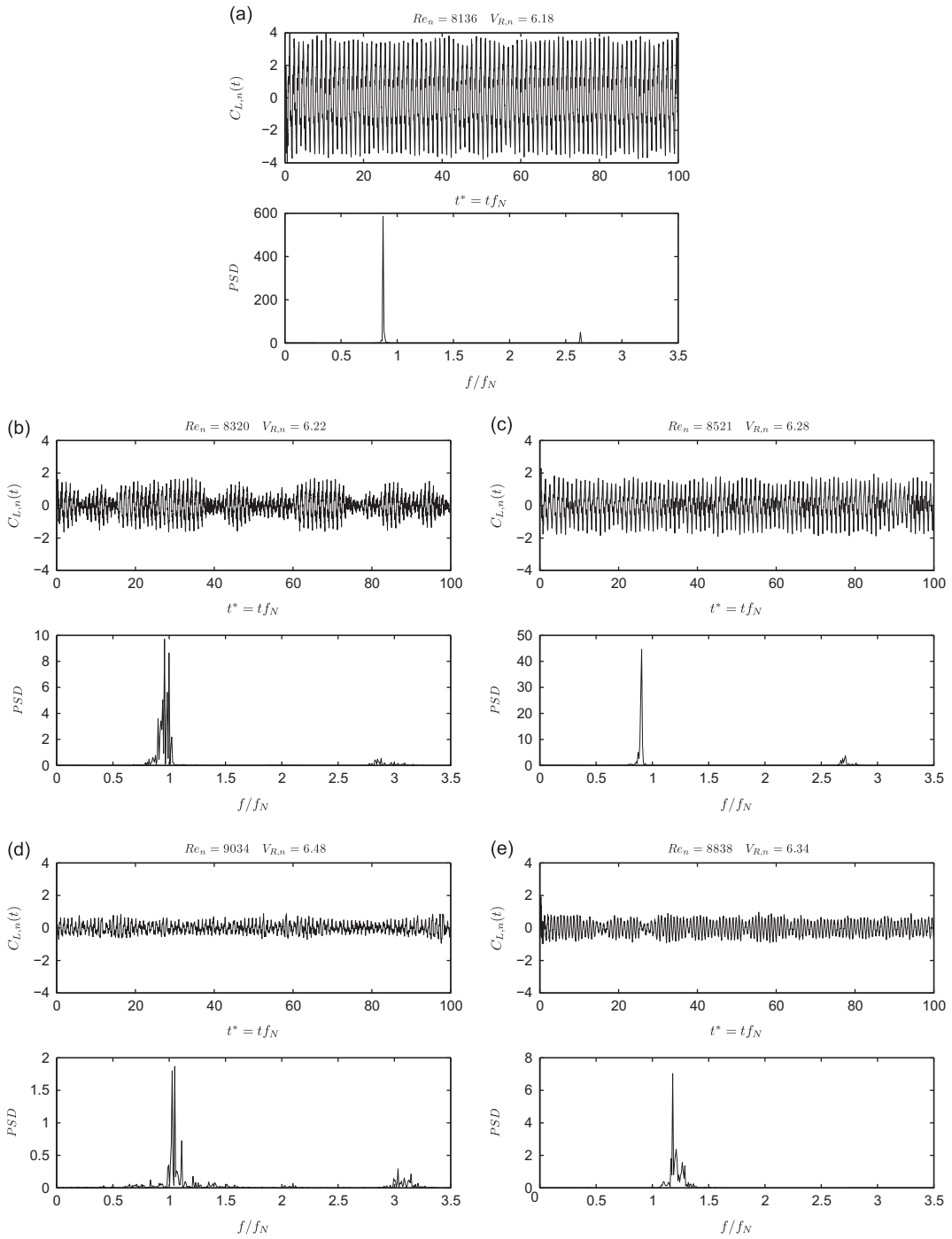

Fig. 15. Lift force time series at $V_{R,n} = 6.2$. 2-dof experiments. (a) $\theta = 0^\circ$, (b) $\theta = -30^\circ$, (c) $\theta = +30^\circ$ and (d) $\theta = -45^\circ$. (e) $\theta = +45^\circ$.

(b) and (d). This fact is in agreement with the paper by Matsumoto et al. (1990), which states that the effect of the axial flow is similar to that of a splitter plate. Hence, the PIV measurements show that the IP may not be sufficient to properly describe the flow around a yawed cylinder in $\theta = -45^\circ$ subjected to VIV.

3.4. Differences between upstream and downstream orientations

Considering both the 1-dof and 2-dof results discussed in the previous subsections, a difference was observed between the results from the upstream and downstream orientations. This difference was monotonic with the increase of the yaw angle.

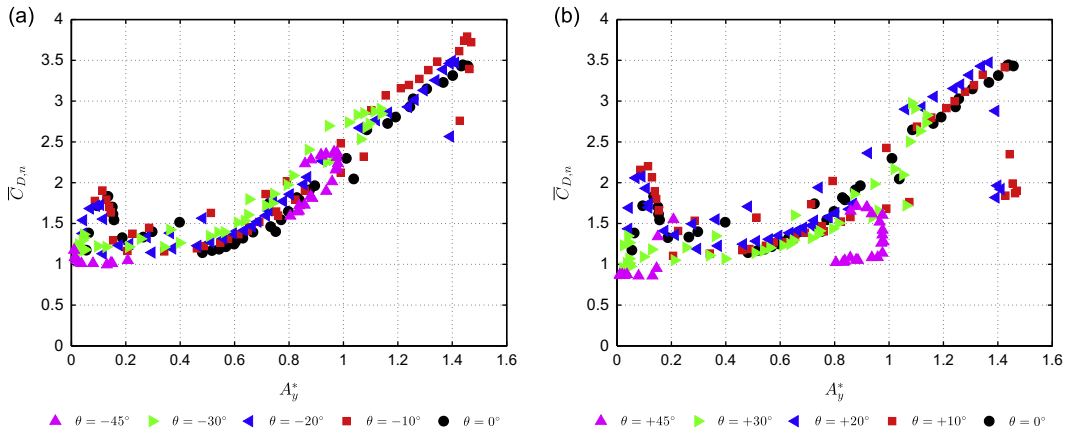

Fig. 16. Mean drag coefficient dependence on the oscillation amplitude. 2-dof experiments. (a) $\overline{C}_{D,n} \times A_y^*$ – upstream and (b) $\overline{C}_{D,n} \times A_y^*$ – downstream.

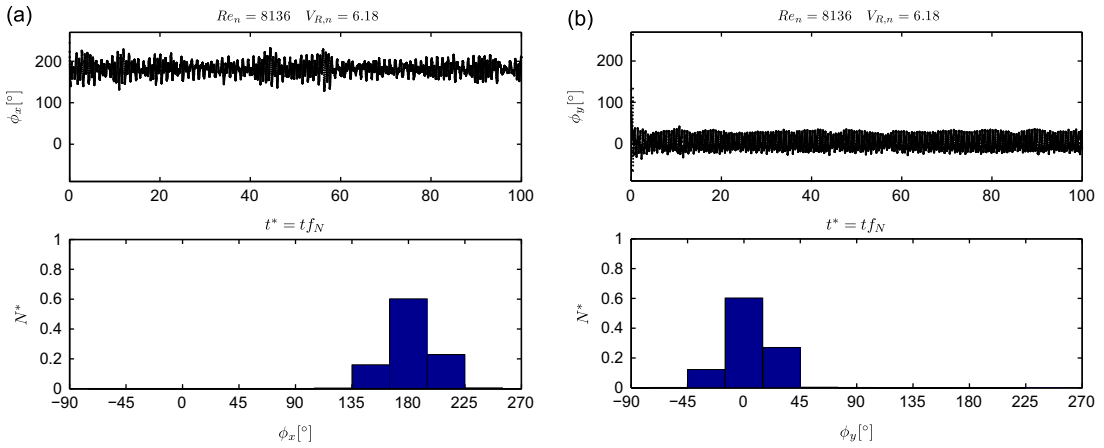

Fig. 17. Phase shift at V_R=6.2 and $\theta = 0°$. 2-dof experiments. (a) Phase shift ϕ_x and (b) phase shift ϕ_y.

As can be found in the literature, the flow around yawed and fixed cylinder is very sensitive to the end conditions of the cylinder, especially those related to the upstream end. The flow visualizations presented in Ramberg (1983), Matsuzaki et al. (2004) and Thakur et al. (2004) showed that the vortex shedding angle near the upstream end can be different from the non-perturbed span. Hogan and Hall (2010, 2011) pointed out that the upstream end of the cylinder enhances the three-dimensional aspects of the flow, with the presence of well organized coherent structures, which can affect the flow along several diameters.

However, the present experimental condition differs from that of those works, because of the presence of two distinct end conditions of the cylinder, since its lower end is very close to the channel floor and its upper end pierces the free surface. In this scenario, the experiments were carried out under similar end conditions with fixed and yawed cylinders presented in Vlachos and Telionis (2008) appear as an enlightening investigation.

According to the above paper, the wake from the cylinder yawed in the upstream orientation is more affected by the flow developed near the bottom end than by the free surface. On the other hand, if the cylinder is yawed in the downstream orientation, the boundary conditions are reversed. The region affected by the bottom end is confined to about one diameter from this end, while the free surface effects are more pronounced. In the downstream orientation, Vlachos and Telionis (2008) observed that the size of the depression formed in the free surface is larger than that from the upstream orientation. Hence, the organization of the wake near the upper end of the cylinder and the reconnection of the vortex with the free surface depend on the orientation of the cylinder.

Owing to the fact that the IP consists of a bidimensional approach, as pointed out by Sears (1948) and Marshall (2003), it is expected that the higher the level of three-dimensional flow is, the weaker the validity of the IP is.

Even though the papers mentioned in this subsection concern visualizations for a fixed cylinder case, the differences observed between the results for the upstream or downstream orientations can be caused by the asymmetric end

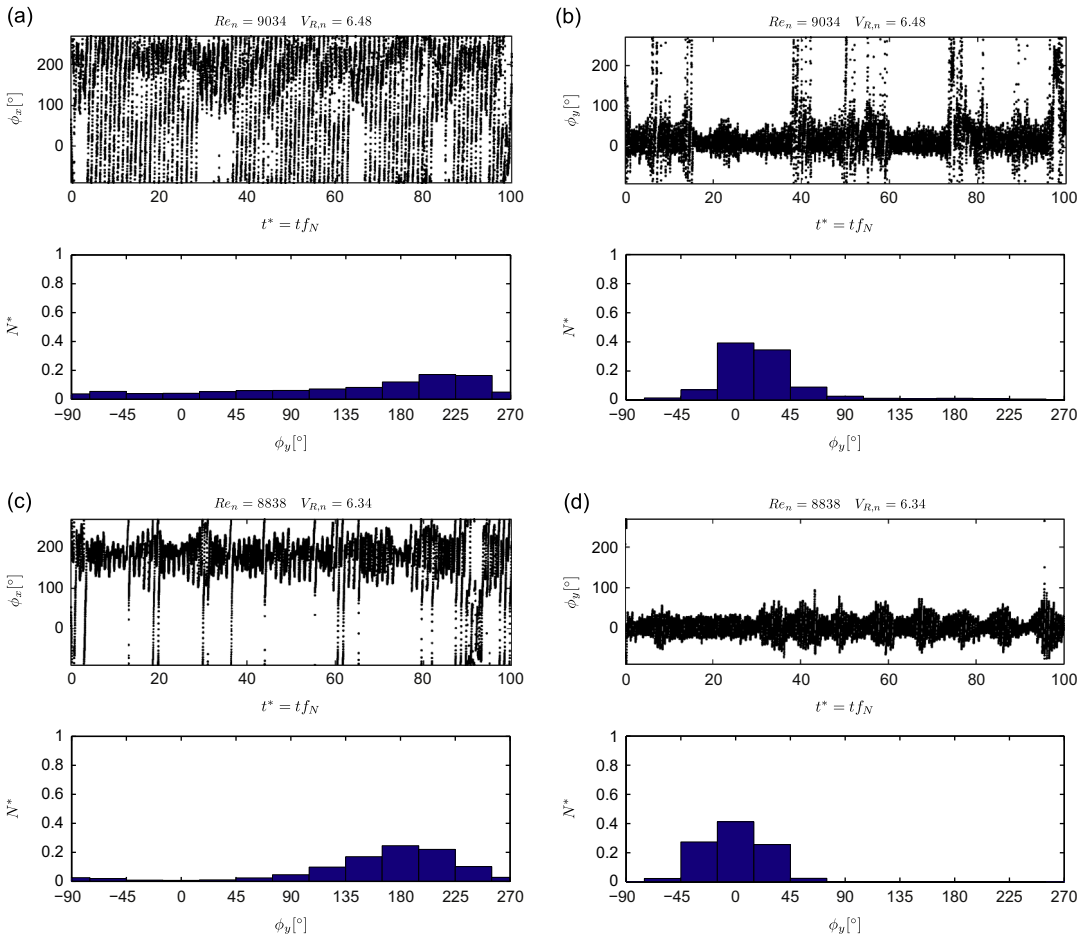

Fig. 18. Phase shift time series at $V_{R,n}$≈6.2 and $\theta = \pm 30^\circ$. 2-dof experiments. (a) ϕ_x – upstream, (b) ϕ_y – upstream, (c) ϕ_x – downstream and (d) ϕ_y – downstream.

conditions of the cylinder. Further flow measurements, as well as numerical simulations may be useful aiming at a better evaluation of the flow around yawed cylinders, especially the flow developed near its ends. It is worth mentioning that the asymmetric end conditions of the cylinder may play an important role in the fluid–structure interaction problem found in the TLP floating platform presented in Williams (2008).

The columns of this kind of structure are characterized by aspect ratio $L/D < 5$. In this scenario, the flow-induced vibration of this structure is characterized by the yaw angle of the columns, the low aspect ratio, the tip vortex and the presence of free surface. Due to the typical aspect ratio values, the effects of the end conditions and, consequently, the differences between upstream and downstream orientations, may be enhanced if compared to those investigated in this work.

Finally, an alternative experimental setup which can be useful aiming at minimizing the differences between upstream and downstream results is that in which a rigid and thin end-plate is attached to the upper end of the cylinder. Notice that this new setup leads to the no-slip condition in both ends and can be better investigated in a future research project.

4. Conclusion

The VIV phenomenon was studied experimentally at a recirculating water channel using rigid and yawed cylinders mounted on elastic base with one and two degrees of freedom, 1-dof and 2-dof respectively, as well as with very low structural damping ζ_s≈0.1%, aspect ratio L/D≈13 and small mass ratio parameter, $m^* = 2.6$. The cylinders were tested in both upstream and downstream orientations for five yaw angles, namely $\theta = 0^\circ, 10^\circ, 20^\circ, 30^\circ$ and 45°, $\theta = 0^\circ$ being the non-yawed case. Oscillation amplitudes and frequencies, force coefficients and phase shift between force and motion were acquired. Despite the numerous researches concerning the VIV on non-yawed cylinders, the problem of the VIV on yawed cylinder has received much less attention, especially in the 2-dof case. In fact, the latter case has no results published in the literature, at least to the authors' knowledge.

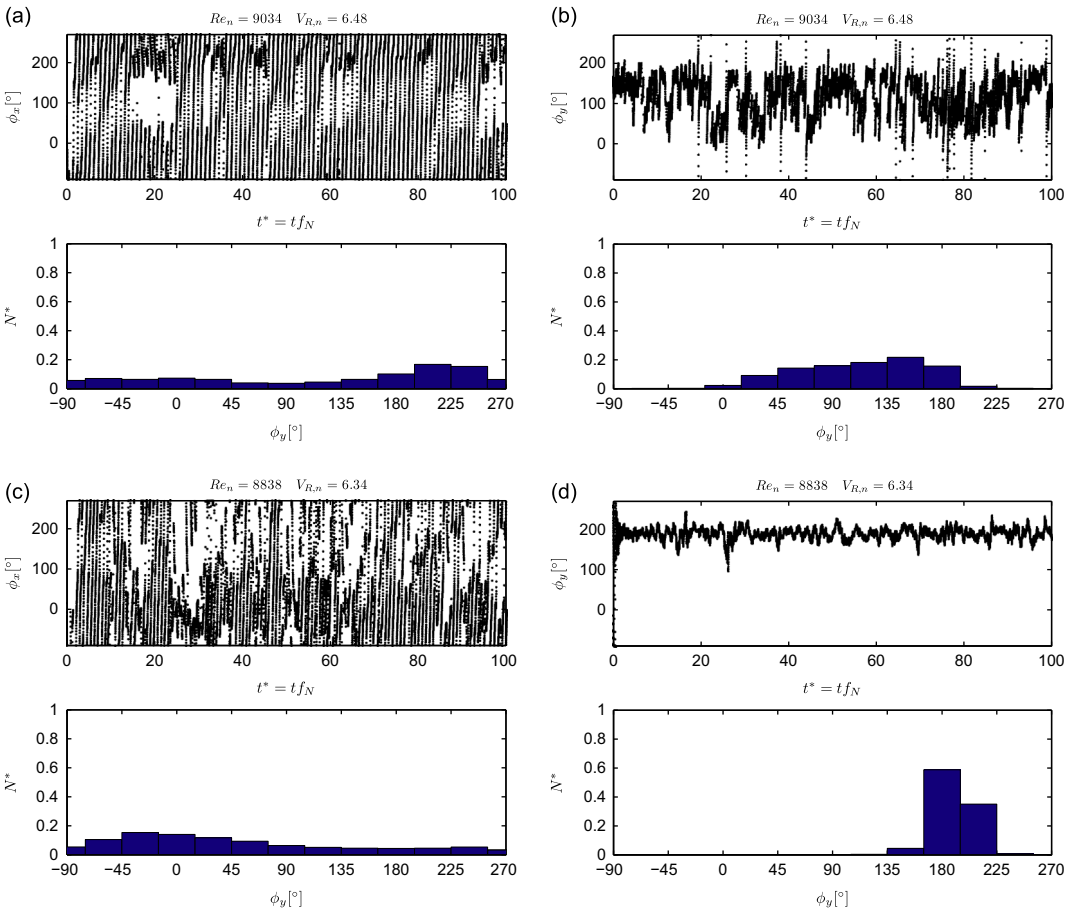

Fig. 19. Phase shift time series at $V_{R,n}$≈6.4 and $\theta = \pm 45^\circ$. 2-dof experiments. (a) ϕ_x – upstream, (b) ϕ_y – upstream, (c) ϕ_x – downstream and (d) ϕ_y – downstream.

For 1-dof and 2-dof experiments, the Independence Principle *IP* was proved to be useful aiming at correcting the range of reduced velocities in which lock-in is observed, in agreement with one degree-of-freedom previous works. On the other hand, the oscillation amplitude decreases with the yaw angle, especially in the 2-dof cases. The increase in the yaw angle leads to a stronger presence of an axial flow, which makes the modulations in the phase shift between force and displacement larger, indicating a less pronounced force-displacement synchronization process. The larger the phase modulation is, the larger the decrease in the oscillation amplitude is.

The IP was also employed in the evaluation of the drag and lift coefficients $C_{D,n}$ and $C_{L,n}$. Considering the 1-dof experiments, the root-mean square lift force coefficient $C'_{L,n}$ matches the results of the non-yawed cylinder for both orientations. Conversely, a marked decrease in the $C'_{L,n}$ plot is observed with the increase in the yaw angle for the 2-dof experiments. For both orientations, the mean drag coefficient $\overline{C}_{D,n}$ decreases with the increase in the yaw angle. However, the relationship between cross-flow amplitude and mean drag coefficient $\overline{C}_{D,n}(A_y^*)$ is independent of the yaw angle for the upstream orientation.

Another effect of the presence of the axial flow is related to the spectral content of the lift force time series obtained from the 2-dof experiments. The $3f_{dy}$ subharmonic, characteristic of the super-upper branch, becomes less defined with the increase of the yaw angle. This fact indicates that the yaw angle affects the fluid excitation and, consequently, the wake characteristics. 2D PIV measurements confirmed that the wake characteristics for the yawed cylinder in $\theta = -45^\circ$ can be significantly different from that observed at $\theta = 0^\circ$ for both 1-dof and 2-dof. All the results indicate that the use of the IP may not be sufficient to correctly describe the Vortex-Induced Vibration of yawed cylinders, especially for yaw angles larger than 20°.

For both 1-dof and 2-dof experiments, differences were observed between the upstream and downstream results. Owing to the high wake sensitivity to the end condition, at least in the case of fixed yawed cylinders, these differences can be associated to the asymmetric end conditions. Flow measurement experiments in other planes along the span may help to properly explain the flow around yawed cylinders subjected to VIV.

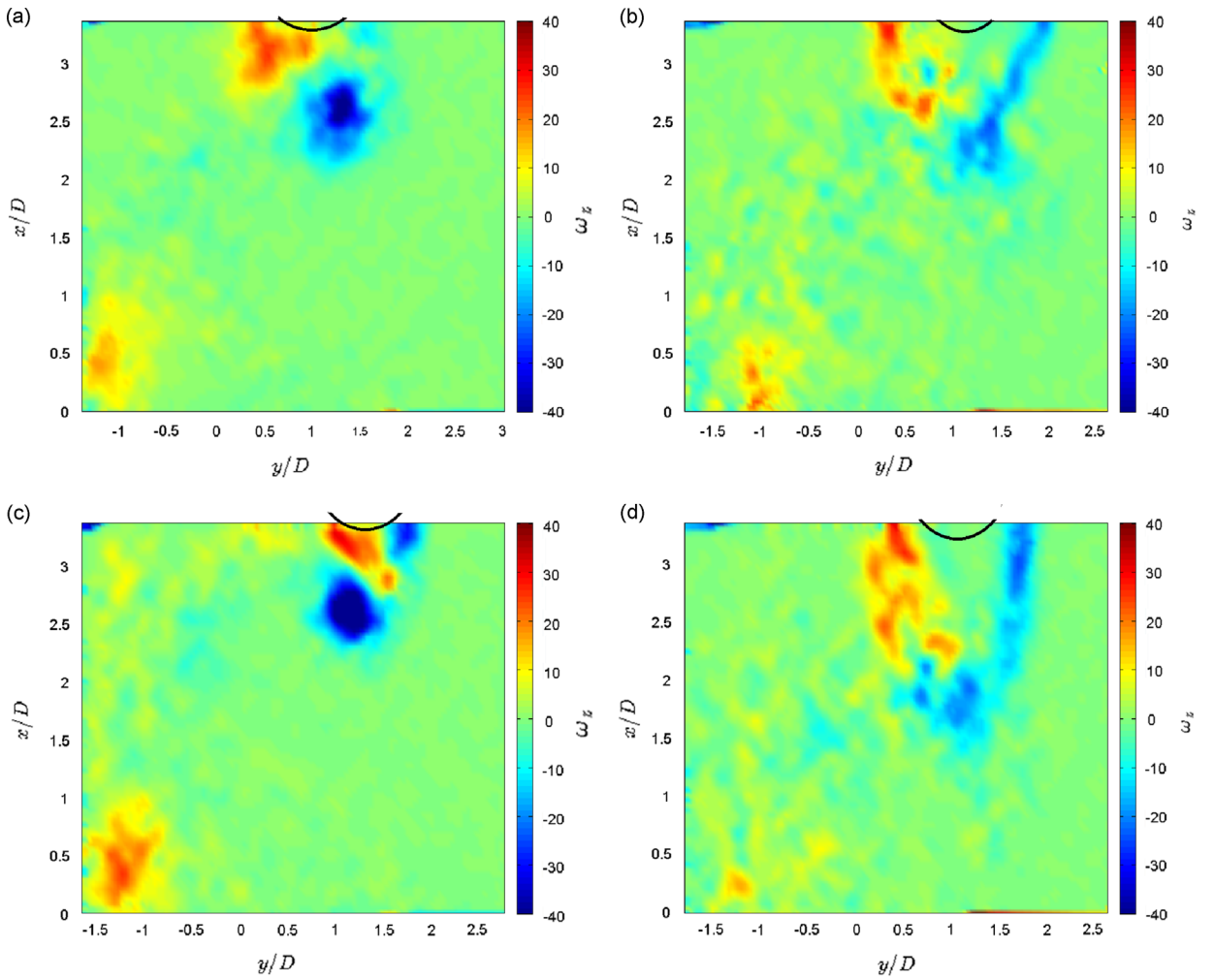

Fig. 20. Phase-averaged out of plane vorticity field ω_z $(1/s)$. $V_{R,n}\approx 6.2$. (a) $\theta = 0^\circ$ and 1-dof, (b) $\theta = -45^\circ$ and 1-dof, (c) $\theta = 0^\circ$ and 2-dof and (d) $\theta = -45^\circ$ and 2-dof.

Acknowledgment

We would like to acknowledge the financial support provided by FINEP, CNPq and FAPESP. G.R.F would like to acknowledge FAPESP for the PhD scholarship (process 2008/00688-4) provided during the development of this work. The authors are also in debt to Prof. Celso P. Pesce, Prof. Clóvis A. Martins and Alfredo Neto for all the useful comments regarding the elastic base design. Special thanks to Cesar Freire, Ivan Korkischko, Douglas Silva, Reinaldo Marcondes Orselli, Rafael Gioria and Pedro Melo for their valuable help with the experiments and the discussion. Prof. Fujarra is grateful to the Brazilian Navy and Maritime Research Institute Netherlands for all the support provided during his sabbatical period, 2011–2012.

References

Assi, G.R.S., Meneghini, J.R., Aranha, J.A.P., Coleto, W.G.P., 2005. Design, assembling and verification of a circulating water channel facility for fluid dynamics experiments. In: Proceedings of the 18th International Congress of Mechanical Engineering, COBEM2005.

Assi, G.R.S., Meneghini, J.R., Aranha, J.A.P., Bearman, P.W., Casaprima, E., 2006. Experimental investigation of flow-induced vibration interference between two circular cylinders. Journal of Fluids and Structures 22, 819–827.

Bearman, P.W., 1984. Vortex shedding from oscillating bluff bodies. Annual Review of Fluids Mechanics 16, 195–222.

Bearman, P.W., 2011. Circular cylinder wake and vortex-induced vibrations. Journal of Fluids and Structures 27, 648–658.

Blevins, R.D., Coughran, C.S., 2009. Experimental investigation of vortex-induced vibration in one and two dimensions with variable mass, damping, and Reynolds number. Journal of Fluids Engineering 131, 1012021–1012027.

Franzini, G.R., Fujarra, A.L.C., Meneghini, J.R., Korkischko, I., Franciss, R., 2009. Experimental investigation of vortex-induced vibration on rigid, smooth and inclined cylinders. Journal of Fluids and Structures 25, 742–750.

Franzini, G.R., Gonçalves, R.T., Meneghini, J.R., Fujarra, A.L.C., 2012a. Comparison between force measurements of one and two degrees-of-freedom VIV on cylinder with small and large mass ratio. In: Proceedings of the 10th FIV 2012 – International Conference on Flow-Induced Vibrations Conference (& Flow-Induced Noise).
Franzini, G.R., Gonçalves, R.T., Meneghini, J.R., Fujarra, A.L.C., 2012b. Experimental investigation into vortex-induced vibrations of yawed cylinders with one and two degrees-of-freedom. In: Proceedings of the 10th FIV 2012 – International Conference on Flow-Induced Vibrations Conference (& Flow-Induced Noise).
Freire, C.M., Meneghini, J.R., 2010. Experimental investigation of VIV on a circular cylinder mounted on an articulated elastic base with two degrees-of-freedom. In: IUTAM Symposium on Bluff Bodies Wakes and Vortex-Induced Vibrations – BBVIV6.
Gabbai, R., Benaroya, H., 2005. An overview of modeling and experiments of vortex-induced vibration of circular cylinders. Journal of Sound and Vibration 282, 575–616.
Gerrard, J.H., 1966. The mechanics of the formation region of vortices behind bluff bodies. Journal of Fluid Mechanics 25, 401–413.
Govardhan, R.N., Williamson, C.H.K., 2006. Defining the "modified Griffin plot" in vortex-induced vibration: revealing the effect of Reynolds number using controlled damping. Journal of Fluid Mechanics 561, 147–180.
Hammache, M., Gharib, M., 1991. An experimental study of the parallel and oblique vortex shedding from circular cylinders. Journal of Fluid Mechanics 232, 567–590.
Hanson, A.R., 1966. Vortex shedding from yawed cylinders. AIAA Journal 4, 738–740.
Hayashi, T., Kawamura, T., 1995. Non-uniformity in a flow around a yawed circular cylinder. Flow Measurement and Instrumentation 6 (1), 33–39.
Hogan, J.D., Hall, J.W., 2010. The spanwise dependence of vortex-shedding from yawed cylinders. Journal of Pressure Vessel Technology 132. 031301-1–031301-5.
Hogan, J.D., Hall, J.W., 2011. Experimental study of pressure fluctuations from yawed circular cylinders. AIAA Journal 49, 2349–2356.
Hover, F.S., Miller, S.N., Triantafyllou, M.S., 1997. Vortex-Induced Vibration of marine cable: experiments using force feedback. Journal of Fluids and Structures 11, 307–326.
Huera-Huarte, F.J., Bearman, P.W., 2009. Wake structures and vortex-induced vibrations of a long flexible cylinder – part 1: dynamic response. Journal of Fluids and Structures 25, 969–990.
Jain, A., Modarres-Sadeghi, Y., 2012. Vortex-induced vibration of an inclined cylinder in flow. In: Proceedings of the 10th FIV 2012 – International Conference on Flow-Induced Vibrations Conference (& Flow-Induced Noise).
Jauvtis, N., Williamson, C.H.K., 2003. Vortex-induced vibration of a cylinder with two degrees of freedom. Journal of Fluids and Structures 17, 1035–1042.
Jauvtis, N., Williamson, C.H.K., 2004. The effect of two degrees of freedom on vortex-induced vibration at low mass and damping. Journal of Fluid Mechanics 509, 23–62.
Jordan, S.A., 2010. Transition to turbulence in the separated shear layers of yawed circular cylinders. International Journal of Heat and Fluid Flow 31, 489–498.
Khalak, A., Williamson, C.H.K., 1997. Fluid forces and dynamics of a hydroelastic structure with very low mass and damping. Journal of Fluids and Structures 11, 973–982.
Khalak, A., Williamson, C.H.K., 1999. Motions, forces and modes transitions in vortex-induced vibration at low Reynolds number. Journal of Fluids and Structures 13, 813–851.
King, R., 1977. Vortex excited oscillations of yawed circular cylinders. Journal of Fluids Engineering 99, 495–502.
Korkischko, I., Meneghini, J.R., 2011. Volumetric reconstruction of the mean flow around circular cylinders fitted with strakes. Experiments in Fluids 51, 1109–1127.
Lucor, D., Karniadakis, G.E., 2003. Effects of oblique inflow in vortex-induced vibrations. Flow, Turbulence and Combustion 71, 375–389.
Marshall, J.S., 2003. Wake dynamics of yawed cylinder. Journal of Fluids Engineering 125, 97–103.
Matsumoto, M., Shiraishi, N., Kitazawa, M., Knisely, C., Shirato, H., Kim, Y., Tsujii, M., 1990. Aerodynamic behavior of inclined circular cylinders – cable aerodynamics. Journal of Wind Engineering and Industrial Aerodynamics 33, 63–72.
Matsuzaki, K., Shingai, M., Haramoto, Y., Munekata, M., Ohba, H., 2004. Visualization of three-dimensional flow structures in the wake of an inclined circular cylinder. Journal of Visualization 7, 309–316.
Moffat, R.J., 1988. Describing the uncertainties in experimental results. Experimental Thermal and Fluid Science 1, 3–17.
Nakagawa, K., Kishida, K., Igarashi, K., 1998. Vortex-induced oscillation and lift of yawed circular cylinders in cross-flow. Journal of Fluids and Structures 12, 759–777.
Norberg, C., 2001. Flow around a circular cylinder: aspects of fluctuating lift. Journal of Fluids and Structures 15, 459–469.
Norberg, C., 2003. Fluctuating lift on a circular cylinder: review and new measurements. Journal of Fluids and Structures 17, 57–96.
Pikovsky, A., Rosenblum, M., Kurths, J., 2001. Synchronization – A Universal Concept in Nonlinear Sciences. Cambridge University Press.
Ramberg, S.E., 1983. The effects of yaw and finite length upon vortex wakes of stationary and vibrating circular cylinders. Journal of Fluid Mechanics 128, 81–107.
Sarpkaya, T., 1995. Hydrodynamic damping, flow-induced oscillations and biharmonic response. Journal of Offshore Mechanics and Arctic Engineering 117, 232–238.
Sarpkaya, T., 2004. A critical review of the intrinsic nature of vortex-induced vibrations. Journal of Fluids and Structures 19, 389–447.
Sears, W.R., 1948. The boundary layer of yawed cylinders. Journal of Aeronautical Sciences 15, 49–52.
Shirakashi, M., Hasegawa, A., Wakiya, S., 1986. Effect of the secondary flow on Kármán vortex shedding from a yawed cylinder. Bulletin of JSME 29, 250–257.
Snarski, S.R., 2004. Flow over yawed circular cylinders: wall pressure spectra and flow regimes. Physics of Fluids 16, 344–359.
Stappenbelt, B., Lalji, F., 2008. Vortex-induced vibration super-upper response branch boundaries. International Journal of Offshore and Polar Engineering 18, 99–105.
Thakur, A., Liu, X., Marshall, J.S., 2004. Wake flow of single and multiple yawed cylinders. Journal of Fluids Engineering 126, 861–870.
Thomson, K.D., Morrison, D.F., 1971. The spacing, position and strength of vortices in the wake of slender cylindrical bodies at large incidence. Journal of Fluid Mechanics 50, 751–783.
van Atta, C.W., 1968. Experiments on vortex shedding from yawed circular cylinders. AIAA Journal 6, 931–933.
Vlachos, P.P., Telionis, D.P., 2008. The effect of free surface on the vortex shedding from inclined circular cylinders. Journal of Fluids Engineering 130. 021103-1–021103-9.
Wang, H.F., Razali, S.F.M., Zhou, T.M., Zhou, Y., Cheng, L., 2011. Streamwise evolution of an inclined cylinder wake. Experiments in Fluids 51, 553–570.
Williams, N., 2008. A deepwater dry-tree GoM solution: the Fourstar TLP. In: Proceedings of the 18th (2008) International Offshore and Polar Engineering Conference – ISOPE 2008.
Williamson, C.H.K., 1989. Oblique and parallel modes of vortex shedding in the wake of a circular cylinder at low Reynolds numbers. Journal of Fluids Mechanics 206, 579–627.
Williamson, C.H.K., Govardhan, R.N., 2004. Vortex-induced vibrations. Annual Review of Fluids Mechanics 36, 413–455.
Williamson, C.H.K., Govardhan, R.N., 2008. A brief review of recent results in vortex-induced vibrations. Journal of Wind Engineering and Industrial Aerodynamics 96, 713–735.
Zhao, M., Cheng, L., Zhou, T., 2009. Direct numerical simulation of three-dimensional flow past a yawed circular cylinder of infinite length. Journal of Fluids and Structures 25, 831–847.
Zhou, T., Razali, S.F.M., Zhou, Y., Chua, L., Cheng, L., 2009. Dependence of the wake on inclination of a stationary cylinder. Experiments in Fluids 46, 1125–1138.